Universitetet i Stavanger

FACULTY OF SCIENCE AND TECHNOLOGY

MASTER'S THESIS

Study programme/specialisation: Petroleum Engineering/ Reservoir Engineering	Spring semester, 2019 Open
Author: Eirik Kjos Nesvik	…… (signature of author)
Faculty Supervisors: Pål Østebø Andersen, Dag Chun Standnes	
Title of master's thesis: Analytical solutions for forced and spontaneous imbibition accounting for viscous coupling	
Credits: 30	
Keywords: Analytical solutions Viscous coupling Relative permeability Generalized model Forced imbibition Spontaneous imbibition	Number of pages: 76 + supplemental material/other: 13 Stavanger, June 14, 2019

Analytical solutions for forced and spontaneous imbibition accounting for viscous coupling

Eirik Kjos Nesvik
University of Stavanger

June 2019

Abstract

Theoretical and experimental work has shown that fluid mobilities can depend on flow configuration, and are typically lower when fluids flow in opposite directions as compared to when they flow in the same direction. Such phenomena are referred to as fluid-fluid interactions or viscous coupling. Conventional modelling of two-phase flow, using simple, saturation dependent relative permeabilities is not able to account for variations in fluid mobilities with flow mode. As measurements are commonly taken during co-current flow, relative permeabilities have to be adjusted manually in order to correctly predict oil recovery in settings that are not purely co-current.

In this work we consider a generalized theory for multiphase flow in porous media based on mixture theory, where fluid mobilities follow from water-rock, oil-rock and water-oil interaction terms defined in momentum equations. The generalized model gives rise to relative permeability expressions that are dependent on the assumed flow mode, as well as fluid viscosities and saturations. By assuming counter-current flow, a new expression for generalized counter-current relative permeabilities has been derived.

The generalized relative permeability expressions have been parametrized against experimental results available in the literature. Further, the expressions have been incorporated into analytical solutions for forced and spontaneous imbibition (SI), to study the effect of viscous coupling during purely co-current and purely counter-current flow. For the case of forced imbibition (FI), the classical Buckley-Leverett theory is used to calculate the solution, while for counter-current SI, the theory by McWhorter and Sunada (1990) using integral solutions is applied.

If viscous coupling is included, the generalized relative permeability expressions indicate that counter-current values are always lower as compared to co-current. In addition, counter-current end point values have been found to be dependent on the viscosity of the opposite phase. Consequently, also the end point values are lower for counter-current flow.

Increased viscous coupling in the FI case led to a more effective displacement, seen as an increase in front saturation and average water saturation behind the front. The same effect was seen for increased water viscosity. Increased oil viscosity led to a less effective process and earlier breakthrough.

For the counter-current SI case, increased viscous coupling resulted in a slowdown of the process, and thus of the oil recovery rate. Increases in viscosities had similar effects. A conventional model will also predict a slowdown of the process for higher viscosities. However, when the generalized model is applied, increased viscosities will additionally depress both oil and water relative permeabilities, resulting in a more significant decrease in imbibition rate. The water-wet media considered here showed higher sensitivity to changes in the water viscosity as compared to oil viscosity. The analytical solutions showed excellent matches to numerical solutions of both a conventional model and the generalized model based on mixture theory. The results suggest that the newly derived relative permeability expressions can be used to construct valid functions if the flow mode is changed from co- to counter-current.

Acknowledgements

I wish to extend my gratitude to my supervisors, Pål Østebø Andersen and Dag Chun Standnes, firstly for suggesting the thesis topic, and giving me the opportunity to build upon their previous work. Secondly for providing excellent help and guidance during this project. Your positive attitudes and feedback has been greatly appreciated.

Also, thanks to my family for providing emotional support!

Contents

List of Figures

List of Tables

Chapter 1

Introduction

1.1 Background

Multiphase flow in porous media is often modelled in terms of relative permeabilities. The common assumption is that the relative permeability is a function of saturation only. Consequently, this standard approach does not account for the role of fluid-fluid interactions between the flowing phases, referred to as viscous coupling. Theory and experimental observations indicate that fluids travelling in opposite directions (counter-currently) experience greater flow resistance and hence lower mobilities compared to when they both travel in the same direction (co-currently) (Babchin et al., 1998; Bentsen and Manai, 1992; Bourbiaux and Kalaydjian, 1990; Dullien and Dong, 1996). Similar phenomena are induced by variations in fluid velocities and viscosities (Armstrong et al., 2017; Ehrlich, 1993; Wang et al., 2006; Odeh, 1959; Nejad et al., 2011). The relative permeabilities measured in the lab are typically from co-current displacements (Geffen et al., 1951; Richardson et al., 1952), and due to the mentioned phenomena, may not transfer directly to counter-current flow settings.

Bourbiaux and Kalaydjian (1990) found that predicting counter-current oil recovery using relative permeabilities determined in a co-current setting led to overestimation of both recovery rate and ultimate oil recovery. Other researcher have demonstrated similar results (Pooladi-Darvish and Firoozabadi, 1998, 2000; Standnes, 2004; Karimaie et al., 2006). This is particularly relevant when scaling up lab results for prediction of oil recovery from naturally fractured reservoirs, where both co- and counter-current spontaneous imbibition can be important recovery mechanisms (Pooladi-Darvish and Firoozabadi, 2000; Mason and Morrow, 2013; Andersen et al., 2014).

While, there is substantial evidence indicating that multiphase flow modelling is more complex than proposed by the simple saturation dependent relative permeability, there is still no agreed upon method of predicting relative permeabilities if the flow mode is changed.

1.2 Objectives

In this work, a generalized model for multiphase flow based on mixture theory is applied. The model gives fluid mobilities that depend on water-rock, oil-rock and water-oil interaction terms, defined in momentum equations. The generalized model gives rise to relative permeability expressions that are dependent on the assumed flow mode. The aim of this work is to extend analytical solutions for forced and spontaneous imbibition to account for viscous coupling phenomena by including such flow mode dependent relative permeabilities. The main objectives of this thesis are as follows:

- Based on the generalized model, derive co- and counter-current relative permeability expressions that can be used in analytical solutions for counter-current SI. The counter-current expressions are derived using a novel approach, that has not been explored in previous works relating to the generalized model.
- Investigate the role of the fluid-fluid interaction term and fluid viscosities on generalized co- and counter-current relative permeabilities.
- Implement analytical solutions for co-current forced imbibition and counter-current spontaneous imbibition accounting for viscous coupling using MATLAB.
- Investigate the role of viscous coupling during co- and counter-current flow by varying input parameters used in the generalized model, such as fluid viscosities and the fluid-fluid interaction parameter that controls the strength of interaction.
- Compare analytical results for the counter-current SI case to numerical solutions of a conventional model and the generalized model. The numerical solution of the generalized model has previously been shown to be able to account for viscous coupling effects as the flow mode is changed.

Chapter 2

Basic theory

2.1 Relative permeability

Relative permeability is one of the key concept for describing multiphase flow through porous media. Extension of Darcy's law (Darcy, 1856) to two-phase flow by incorporation of relative permeabilities was presented by Muskat et al. (1937). The phase fluxes for a one-dimensional oil-water system using their approach can be written in the following way:

$$u_i = -\frac{kk_{ri}}{\mu_i}\frac{\partial p_i}{\partial x}, \quad (i = o, w). \tag{2.1}$$

Here, u_i is phase flux or Darcy velocity of phase i, k is the absolute permeability of the porous medium, k_{ri} is the relative permeability to phase i, μ_i is the phase viscosity and $\partial p_i/\partial x$ is the pressure gradient in the x-direction. The relative permeability can be viewed as the fraction of the absolute permeability that is available for the phase in question. Hence, a higher value for relative permeability will equate to lower flow resistance and higher flow rate.

2.1.1 Measuring relative permeability

Experimental methods for determination of relative permeability can be divided into two main types: steady-state and unsteady-state. The most common and simplest methods are based on steady-state flow, and all follow essentially the same procedure (Bear, 2013): Oil and water is injected at a certain ratio at the inflow end of a core sample. Enough time is then allowed to pass, such that a steady flow has developed, where the inflow ratio equals the outflow ratio. The pressures in each phase at both ends is measured, and the flow rates and saturations are determined. Relative permeabilities for oil and water at the current saturations can then be calculated from Eq. (2.1). By varying the ratio of oil and water that is injected, a set of points is obtained, which can be used to construct complete relative permeability curves.

Unsteady-state methods are significantly quicker, due to not requiring saturation equilibrium to be reached, but also more mathematically complicated, involving the use of Buckley-Leverett-theory to compute relative permeabilities (Anderson, 1987;

Honarpour and Mahmood, 1988; Richardson et al., 1952). Exact experimental procedures will not be covered in any more detail, as it is not directly relevant for this thesis. However, one key aspect regarding measurements of relative permeability is very much relevant for this work. This is the notion that standard measurements are taken during co-current flow, where both fluids are flowing in the same direction. Hence, resulting relative permeabilities might not be representative for settings where counter-current flow is significant. This will be covered in more detail in Chapter 3, where the concept of viscous coupling is explained.

2.1.2 Simple relative permeability models

Several mathematical models for correlation of relative permeabilities have been presented through the years. In this work, a simple power-law model is applied to describe relative permeabilities as functions of phase saturations. The relations are as follows:

$$k_{rw} = k_{rw}^{max}(S_w)^{n_w}, \tag{2.2}$$

$$k_{ro} = k_{ro}^{max}(1 - S_w)^{n_o}, \tag{2.3}$$

where k_{rw}^{max} and k_{ro}^{max} represent end point relative permeabilities for water and oil, respectively, S_w is normalized water saturation, and n_w and n_o are saturation exponents for water and oil. The saturation exponents control the shape of the relative permeability curves, and can thus be used for curve fitting. Simple models of this form are often referred to as modified Brooks-Corey expressions, due to their similarity to expressions presented by Brooks and Corey (1964). In this thesis, relative permeabilities of the form shown in (2.2) and (2.3) will be referred to as "Corey-type".

2.1.3 Impact of wettability

Wettability describes the tendency of one fluid to adhere to a solid surface in the presence of other immiscible fluids (Craig, 1971). In a strongly water-wet porous media, which is what will be considered in this work, the solid is preferentially coated by water. This affects the distribution of fluids in the pore space, where water will occupy the pore walls and the smaller pores, while oil can be found in the middle of larger pores. This difference in fluid distribution is illustrated in Fig. 2.1.

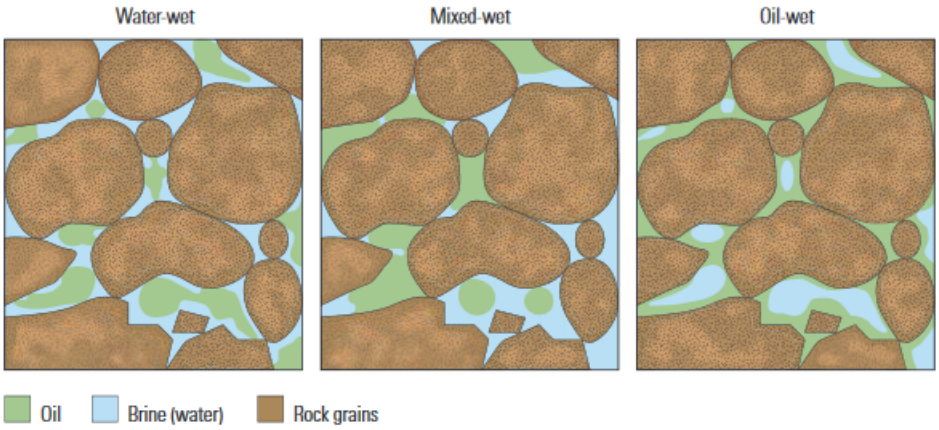

Figure 2.1: Illustration of fluid distribution in the pore space of water-wet, mixed-wet and oil-wet rock. From (Abdallah et al., 2007).

At water saturations near the residual water saturation, the water has little effect on the flow of oil, and the oil effective permeability can approach the absolute permeability. Conversely, near residual oil saturation, the oil that is trapped in larger pores can block the flow of water. This leads to a low relative (and effective) permeability for water at the end point. Fig. 2.2 illustrates the characteristic differences seen in relative permeabilities for water-wet and oil-wet porous media.

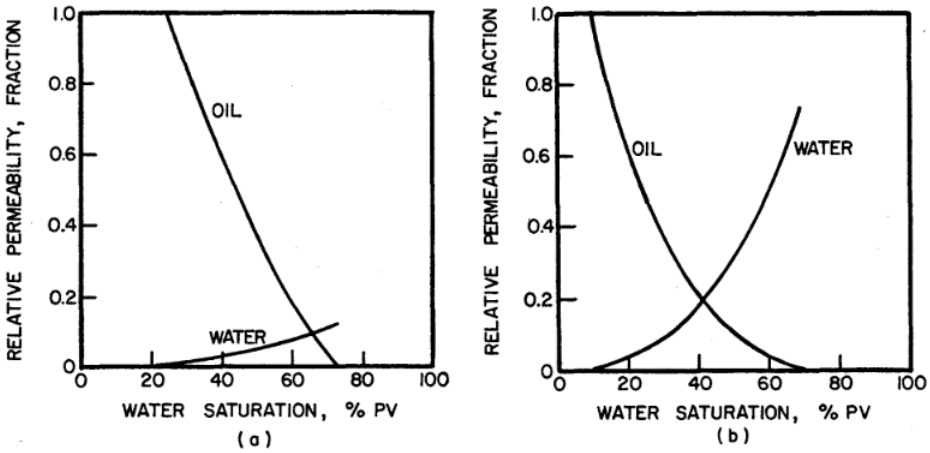

Figure 2.2: Illustration of typical relative permeability curves for (a): water-wet porous media, (b): oil-wet porous media. From Anderson (1987).

For the oil-wet case, the situation is reversed. As water saturation increases, the water will start to fill the larger pores, thus blocking the flow of oil. As the oil approaches resiudual oil saturation, it will have little effect on the flow of water. Consequently, the end point relative permeability for water is much higher for the oil-wet case (Anderson, 1987).

2.2 Capillary pressure

Capillary pressure is another phenomenon that is related to differences in adhesive forces between fluids and the solid porous medium. It can be defined as the pressure difference across a curved interface between two immiscible fluids. The capillary pressure, p_c, is given by the Laplace equation:

$$p_c = p_o - p_w = \sigma_{ow}\left(\frac{1}{R_1} + \frac{1}{R_2}\right), \tag{2.4}$$

where p_o and p_w are pressures in the oil and water phases, respectively, σ_{ow} is interfacial tension between oil and water, R_1 and R_2 are principal radii of curvature. If a capillary tube is used as a simplified representation of a single pore in a porous medium, the capillary pressure can be expressed as

$$p_c = p_o - p_w = \frac{2\sigma_{ow} \cdot \cos\theta}{R_{tube}}, \tag{2.5}$$

where θ represents the contact angle at the interface, which is related to the wettability of the system and R_{tube} is the radius of the capillary tube, as illustrated in Fig. 2.3. The figure illustrates a case where the capillary tube is preferentially water-wet. Due to the difference in adhesive forces between the two fluids and the solid surface, water is able to rise above the water level outside of the tube. This also happens in a real world reservoir, and thus affects the fluid saturation distribution in a transition zone above the free water level (for a water-wet reservoir).

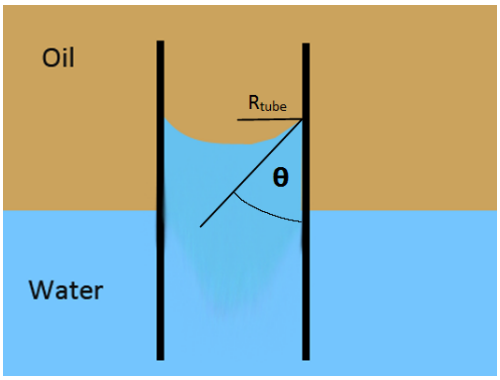

Figure 2.3: Illustration of oil/water interface in a capillary tube.

2.2.1 Spontaneous imbibition

A displacement process where the wetting phase saturation is increasing is referred to as an imbibition process. When water displaces oil due to capillary pressure, the process is called spontaneous imbibition (SI). Fig. 2.4 illustrates a capillary pressure curve for a water-wet porous medium, such as the one that will be considered in this thesis. The key characteristic to take note of is that for a water-wet medium, the capillary pressure is assumed positive for the whole saturation range where oil is mobile (i.e. from s_{wr} to $1 - s_{or}$) (Schmid and Geiger, 2013).

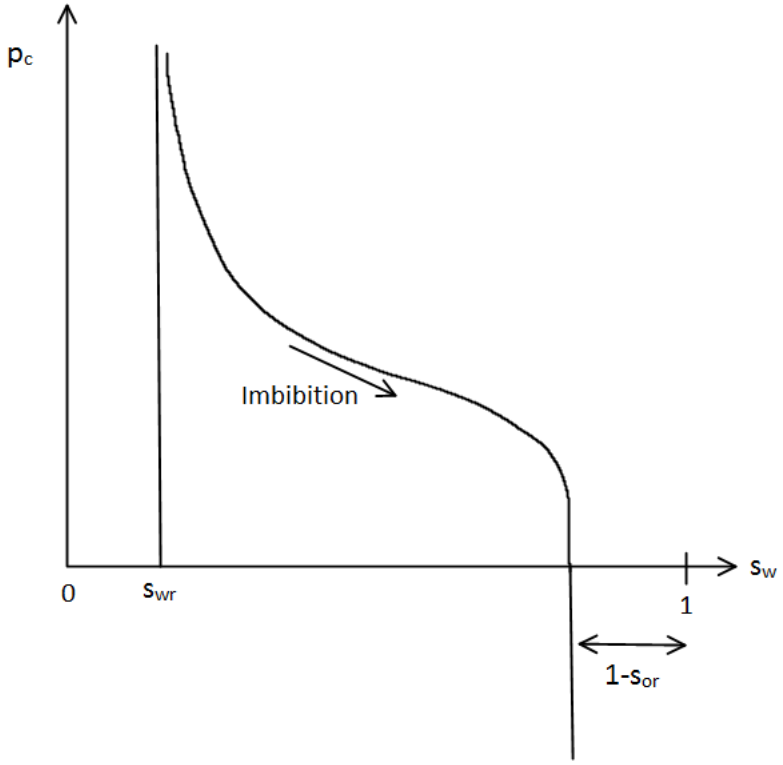

Figure 2.4: Illustration of capillary pressure curve for imbibition in a water-wet porous medium.

2.2.2 Capillary pressure correlation

Several mathematical expressions exist for correlating capillary pressure curves as functions of water saturation. In this work it is assumed that the capillary pressure follows the Leverett J-function scaling (Bear, 2013; Leverett, 1941):

$$p_c = \sigma_{ow}\sqrt{\frac{\phi}{k}}J(S_w), \tag{2.6}$$

where σ_{ow} is interfacial tension between oil and water, ϕ is porosity, k is the absolute permeability of the porous medium and $J(S_w)$ is a dimensionless capillary pressure

function. The advantage of using a model of this type is that it can be used to correlate capillary pressure for rocks with similar pore structure and wettability, but different permeability. For the dimensionless function $J(S_w)$, the following expression by Andersen et al. (2014, 2017a) is used :

$$J(S_w) = \frac{a_1}{1 + k_1 S_w} - \frac{a_2}{1 + k_2(1 - S_w)} + c, \tag{2.7}$$

where $a_1, a_2, k_1, k_2 > 0$ and c are curve-fitting parameters. The same expression was applied in other works which relate closely to this thesis (Andersen et al., 2019; Qiao et al., 2018).

2.3 1D mass balance equations

Consider a control volume V of the reservoir of length Δx and cross sectional area A_c, such that $V = A_c \Delta x$, as illustrated in Fig 2.5. Let $u(x,t)$ represent fluid flux,

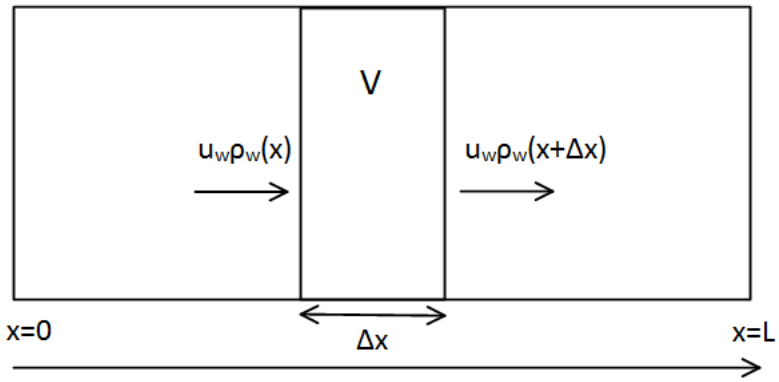

Figure 2.5: Illustration of mass flow into and out of the control volume V.

$\phi(x,t)$ porosity and $\rho(x,t)$ fluid density. Assume also that water is injected from the left hand side of the reservoir, resulting in rightward flow. Let t represent a point in time and Δt a small time increment. Mass flow of water into V at position x during a time interval Δt is then given by

$$A_c u_w(x) \rho_w(x) \Delta t, \tag{2.8}$$

where the product $A_c u_w$ represents volumetric flow rate. Mass flow of water out of V at position $x + \Delta x$ is similarly given by

$$A_c u_w(x + \Delta x) \rho_w(x + \Delta x) \Delta t. \tag{2.9}$$

The change in water mass in V is equal to

$$[u_w(x)\rho_w(x) - u_w(x + \Delta x)\rho_w(x + \Delta x)] A_c \Delta t \tag{2.10}$$

Change of water mass can also be expressed as

$$V[\phi(t + \Delta t)\rho_w(t + \Delta t)S_w(t + \Delta t) - \phi(t)\rho_w(t)S_w(t)] \tag{2.11}$$

Here we assume an incompressible reservoir and incompressible fluids. From these assumptions, it follows that densities and porosity are constant values, independent

of position and time. Using this, the expression in (2.10) simplifies to:

$$[u_w(x) - u_w(x + \Delta x)]\rho_w A_c \Delta t \tag{2.12}$$

Similarly, (2.11) is simplified:

$$\rho_w \phi V[S_w(t + \Delta t) - S_w(t)] \tag{2.13}$$

The expressions both represent the change of mass in the control volume V, and must be equal.

$$[u_w(x) - u_w(x + \Delta x)]\rho_w A_c \Delta t = \rho_w \phi V[S_w(t + \Delta t) - S_w(t)] \tag{2.14}$$

Dividing both sides by $\rho_w A_c \Delta x \Delta t$, and noting that $V = A_c \Delta x$, gives:

$$\frac{u_w(x) - u_w(x + \Delta x)}{\Delta x} = \frac{\phi[S_w(t + \Delta t) - S_w(t)]}{\Delta t} \tag{2.15}$$

We then recall the definition of a derivative:

$$f' = \lim_{h \to 0} \frac{f(x + h) - f(x)}{h}. \tag{2.16}$$

In this definition f is an arbitrary, smooth function and h is a small jump along the x-axis. Letting Δx and Δt in (2.15) approach zero, and by applying the definition of a derivative, the differential equation for mass conservation (for water in this case) is obtained:

$$\frac{\partial u_w}{\partial x} = -\phi \frac{\partial S_w}{\partial t} \tag{2.17}$$

Using the same method for mass conservation of oil yields the corresponding oil equation:

$$\frac{\partial u_o}{\partial x} = -\phi \frac{\partial S_o}{\partial t} \tag{2.18}$$

Chapter 3

Generalized modeling of two-phase flow.

3.1 Limitations of the conventional Darcy model.

The conventional way of modelling two-phase flow in porous media, as described by extension of Darcy's law in Eq. (2.1), relies on the major assumption that a fluids relative permeability is only a function of its own phase saturation. Consequently, conventional relative permeability curves cannot account for different types of flow configurations, as they do not include the velocity or pressure of the other phase. The relative permeability that results from experimental measurements can be thought of as a system specific representation of several different effects governing two-phase flow, all lumped into one number. Hence, there is no account for variation in interaction between the fluids or between fluid and rock if the flow setting is changed from co-current to counter-current, or some combination of the two. To get around this limitation and ensure applicability of lab results, measurements of relative permeabilities should ideally be performed under conditions similar to those expected in the reservoir.

3.2 Viscous coupling.

The term viscous coupling refers to fluid-fluid interactions during multi-phase flow in porous media. Yuster (1951) first mentioned such phenomena after theoretical analysis of two-phase flow in capillary tubes. He found that relative permeabilities should not only depend on saturations, but also on the viscosity ratio of the fluid phases. Subsequent research has indicated that relative permeabilities are dependant on saturation, capillary number and viscosity ratio (Armstrong et al., 2017; Avraam and Payatakes, 1995a; Ehrlich, 1993). Additionally, experimental work by Bourbiaux and Kalaydjian (1990), Bentsen and Manai (1992) and Dullien and Dong (1996) has suggested that the relative flow direction of the phases is important to take into consideration.

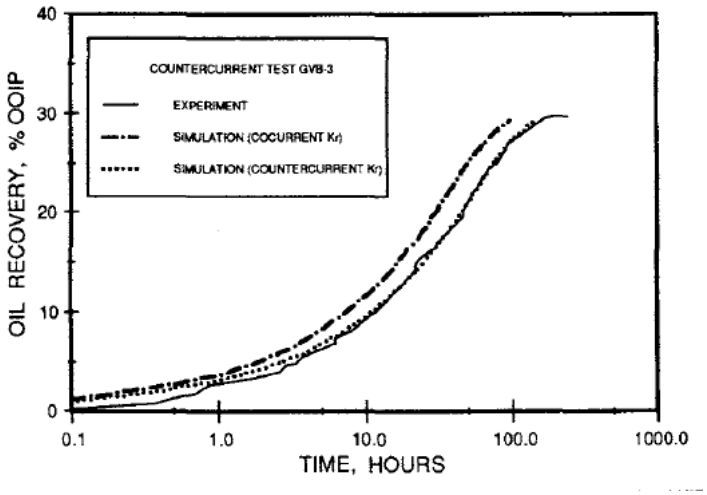

Figure 3.1: Oil recovery for simulations using co-current and counter-current relative permeabilities compared to experimental result GVB-3. From Bourbiaux and Kalaydjian (1990).

Bourbiaux and Kalaydjian (1990) performed experiments on a natural, low permeability porous medium, representative of the matrix blocks in fractured reservoirs. The material was strongly water-wet to ensure that capillary pressure served as a driving force for spontaneous imbibition. Their experiments with counter-current imbibition showed slower oil recovery, a smoother front and slightly lower ultimate oil recovery when compared to those where the flow was mainly co-current. Additionaly, they performed numerical simulations using relative permeability curves based on a co-current imbibition experiment to simulate counter-current imbibition. This resulted in overestimation of imbibition rate when compared to their counter-current experiment, as can be seen in figure 3.1. In particular, the half-recovery time was underestimated by about 25% when co-current curves were used. By modifying the co-current relative permeabilities, they were able to match their counter-current experimental result. They noted that a good match was obtained by decreasing oil relative permeabilities by 60% of the co-current values, water (brine) relative permeabilities by 45% of their co-current values, or both by around 30%. The original co-current curves and reduced curves that resulted in good prediction are shown in Fig. 3.2.

Bentsen and Manai (1992) performed steady-state experiments involving two-phase co- and counter-current flow in a 1-D, horizontal, unconsolidated porous medium. Their measurements of saturation and pressure distribution along the core were used to estimate relative permeability and capillary pressure curves for both flow modes. The magnitude of a counter-current relative permeability at a given saturation was found to always be less than that of a corresponding co-current relative permeability. For the wetting phase the relative difference was always greater than 25%, while for the non-wetting phase it was always greater than 20%.

Several generalized equations that take into account fluid-fluid interactions have been presented in the literature. The common feature that characterizes models of this form is the incorporation of four mobility terms instead of the two used in

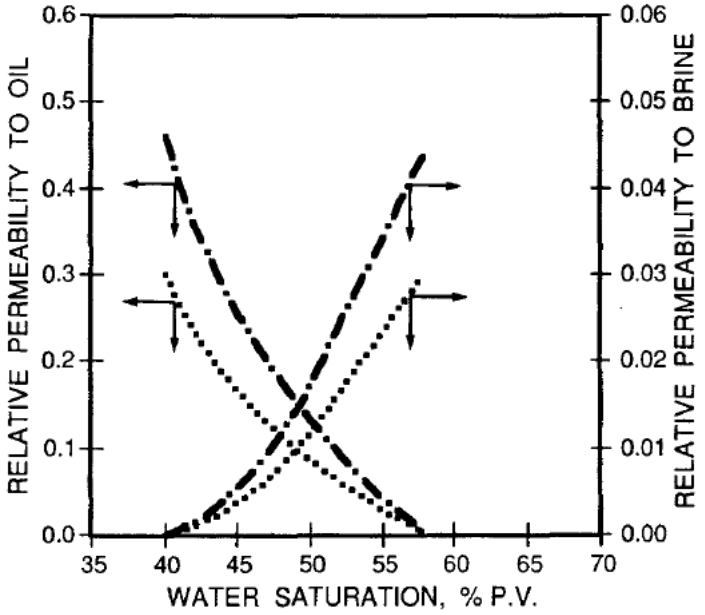

Figure 3.2: Comparison between co-current relative permeability curves and reduced curves used in simulation to match counter-current experiment GVB-3. From Bourbiaux and Kalaydjian (1990).

conventional Darcy models. They can be expressed in the general form (Standnes et al., 2017):

$$u_w = -\lambda_{ww}\frac{\partial p_w}{\partial x} - \lambda_{wo}\frac{\partial p_o}{\partial x} \tag{3.1}$$

$$u_o = -\lambda_{ow}\frac{\partial p_w}{\partial x} - \lambda_{oo}\frac{\partial p_o}{\partial x}, \tag{3.2}$$

where $\lambda_{ij}(i, j = w, o)$ are referred to as generalized phase mobilities. From this it can be seen that the water flux is not only dependent on water mobility (λ_{ww}) and the pressure gradient in the water phase, but also on a cross-term mobility (λ_{wo}) and the pressure gradient in the oil phase. Similarly, the oil flux includes a cross-term mobility and the pressure gradient in the water phase.

Avraam and Payatakes (1995b) investigated the role of the cross-terms experimentally in 2-D micro models in steady-state, co-current flow of water and oil. They concluded that viscous coupling is important over broad ranges of wetting phase saturation, capillary number and viscosity ratio. Dullien and Dong (1996) measured cross-terms over wide water saturation ranges in sand packs using a fluid system with viscosity ratio of unity. The values of the cross terms were found to be significant, ranging from 10 to 35% of the value of the effective permeability to water and from 5 to 15 % of the effective permeability to oil, respectively.

3.3 Derivation of the model based on mixture theory.

The generalized model that is applied to account for viscous coupling is based on extension of the theory of mixtures to porous media (Bowen, 1980; Rajagopal and Tao, 1995; Ambrosi and Preziosi, 2002). The idea behind the model is that the pressure gradient over each fluid phase is related to friction between fluid and rock, as well as drag between the fluids at the fluid-fluid interface. Detailed derivations of the model and description of the numerical schemes can be found in previous works by Standnes et al. (2017) and Qiao et al. (2018). They derived the model for 3-D flow with gravity included. As the model is relatively new, and plays a key role for this work, it is repeated here. The following is an outline of the generalized model in its simplest form (no source term, no gravity), based on the work of Andersen et al. (2019) Andersen et al. (2018). It is key to understanding the difference between the numerical solutions used for comparison against the analytical solutions for counter-current SI. The model is also the basis for the new generalized relative permeabilities for counter-current SI that are derived in a later section.

1D mass balance equations for horizontal, incompressible transport of water and oil are given by:

$$\frac{\partial(\phi s_i)}{\partial t} + \frac{\partial u_i}{\partial x} = 0, \qquad (i = w, o) \tag{3.3}$$

$$u_i = \phi(s_i - s_{wr})v_i, \tag{3.4}$$

where ϕ is porosity, s_i fluid saturation, s_{wr} residual water saturation and v_i is interstitial fluid velocity. The latter equation expresses the relation between flux and interstitial valocity in the mobile domain. For simplicity, an effective porosity is introduced:

$$\phi_e = \phi(1 - s_{or} - s_{wr}) \tag{3.5}$$

This allows us to write

$$u_i = \phi_e S_i v_i, \qquad (i = w, o), \tag{3.6}$$

$$S_w = \frac{s_w - s_{wr}}{1 - s_{or} - s_{wr}}, \tag{3.7}$$

where S_w is normalized. The saturations must add to unity due to conservation of volume:

$$S_w + S_o = 1, \tag{3.8}$$

and the capillary pressure relating the phase pressures is assumed:

$$p_c = p_o - p_w. \tag{3.9}$$

These equations are so far in line with conventional modeling using the extension of Darcy's law. For the generalized model the approach based on Darcy's law is replaced by a coupled momentum equation model. Ignoring inertial effects, as is usual for creeping (slow) flow in porous media, the mechanical stress balance for a fluid is given by (Ambrosi and Preziosi, 2002):

$$\frac{\partial(S_i\sigma_i)}{\partial x} + m_i = 0 \qquad (i = w, o), \tag{3.10}$$

where σ_i represents the Cauchy stress tensor and m_i represents interaction forces exerted on fluid i by the other constituents of the mixture. In 1-D, the standard expression for the stress term is:

$$\sigma_i = -p_i + \tau_i \qquad (i = w, o), \tag{3.11}$$

where τ_i represents viscous forces. In the following the contribution from τ_i is ignored ($\tau_i = 0$). The interaction forces m_i are given by (Preziosi and Farina, 2002; Ambrosi and Preziosi, 2002):

$$m_w = p_w \frac{\partial S_w}{\partial x} - F_{ow} + M_{wm} \tag{3.12}$$

$$m_o = p_o \frac{\partial S_o}{\partial x} + F_{ow} + M_{om}, \tag{3.13}$$

where F_{ow} represents the drag force exerted by the water phase on the oil phase. The oil must necessarily exert an equal and opposite force, $-F_{ow}$, on the water phase. The terms M_{om} and M_{wm} denote interaction forces between the fluids and the porous media for oil and water, respectively. The terms $p_w \partial S_w/\partial x$ and $p_o \partial S_o/\partial x$ represent interfacial forces arising from an averaging process. The drag force is modeled as (Preziosi and Farina, 2002; Ambrosi and Preziosi, 2002):

$$F_{ow} = R(v_w - v_o). \tag{3.14}$$

Thus, the force exerted between the fluids is related to the difference in interstitial velocities through a fluid-fluid interaction term, $R \geq 0$, which needs further specification. Similarly, the force between a fluid and the matrix wall is expressed as:

$$M_{im} = -R_i v_i \qquad (i = w, o), \tag{3.15}$$

where the interaction terms R_i are assumed larger than or equal to zero ($R_i \geq 0$). Combination of Eqs. (3.10) through (3.15), where the chain rule is applied to Eq.

(3.10) and $\tau_i = 0$, results in:

$$S_w \frac{\partial p_w}{\partial x} = -R_w v_w + R(v_o - v_w) \tag{3.16}$$

$$S_o \frac{\partial p_o}{\partial x} = -R_o v_w - R(v_o - v_w), \tag{3.17}$$

where the right hand side of the equations represent matrix-fluid and fluid-fluid interaction. Solving for the interstitial velocities and inserting these into (3.6), yields:

$$u_w = -\hat{\lambda}_{ww} \frac{\partial p_w}{\partial x} - \hat{\lambda}_{wo} \frac{\partial p_o}{\partial x}, \tag{3.18}$$

$$u_o = -\hat{\lambda}_{ow} \frac{\partial p_w}{\partial x} - \hat{\lambda}_{oo} \frac{\partial p_o}{\partial x}. \tag{3.19}$$

A key observation here is that the expressions for the fluxes are of the form presented in Eqs. (3.1) and (3.2), using generalized mobilities. If the capillary pressure relation $p_c = p_o - p_w$ is used we have:

$$u_w = -(\hat{\lambda}_{ww} + \hat{\lambda}_{wo}) \frac{\partial p_w}{\partial x} - \hat{\lambda}_{wo} \frac{\partial p_c}{\partial x}, \tag{3.20}$$

$$u_o = -(\hat{\lambda}_{ow} + \hat{\lambda}_{oo}) \frac{\partial p_w}{\partial x} - \hat{\lambda}_{oo} \frac{\partial p_c}{\partial x}. \tag{3.21}$$

With the following definitions for generalized diagonal and cross-term mobilities:

$$\hat{\lambda}_{ww} = \frac{{S_w}^2 (R_o + R)}{R_o R_w + R(R_o + R_w)} \phi_e, \tag{3.22}$$

$$\hat{\lambda}_{oo} = \frac{{S_o}^2 (R_w + R)}{R_o R_w + R(R_o + R_w)} \phi_e, \tag{3.23}$$

$$\hat{\lambda}_{ow} = \hat{\lambda}_{wo} = \frac{S_w S_o R}{R_o R_w + R(R_o + R_w)} \phi_e. \tag{3.24}$$

The following notation is defined for generalized phase mobilities $\hat{\lambda}_w, \hat{\lambda}_o$ and total mobility $\hat{\lambda}_T$:

$$\hat{\lambda}_w = \hat{\lambda}_{ww} + \hat{\lambda}_{wo} = \frac{{S_w}^2 R_o + S_w R}{R_o R_w + R(R_o + R_w)} \phi_e, \tag{3.25}$$

$$\hat{\lambda}_o = \hat{\lambda}_{ow} + \hat{\lambda}_{oo} = \frac{{S_o}^2 R_w + S_o R}{R_o R_w + R(R_o + R_w)} \phi_e, \tag{3.26}$$

$$\hat{\lambda}_T = \hat{\lambda}_o + \hat{\lambda}_w = \frac{{S_w}^2 R_o + S_o R_w + R}{R_o R_w + R(R_o + R_w)} \phi_e. \tag{3.27}$$

Here it is assumed that the fluid-fluid interaction terms (denoted R_{wo} when water is acting on oil and R_{ow} when oil is acting on water) are equal, hence $R_{wo} = R_{ow} = R$. This leads to equality of the cross-terms $\hat{\lambda}_{wo} = \hat{\lambda}_{ow}$, and implies validity of Onsager's reciprocal relationship (Onsager, 1931). Note that the hat notation is used to signify that the mobilities (and later permeabilities) are expressed using generalized interaction parameters. The terms R and R_i characterize the magnitude of fluid-fluid and rock-fluid interaction. Typically, R should be proportional to the product kS_wS_o to reflect that the term vanishes if one of the phase saturations is zero. If $R = 0$ is used, with the interpretation that fluid-fluid interaction is zero, we get the following phase fluxes:

$$u_w = -\frac{{S_w}^2}{R_w} \phi_e \frac{\partial p_w}{\partial x}, \qquad u_o = -\frac{{S_o}^2}{R_o} \phi_e \frac{\partial p_o}{\partial x}. \tag{3.28}$$

Notably, the fluid flux now only depends on its own saturation and pressure gradient, in addition to the solid-fluid interaction term. This term can be chosen such that the conventional model based on extension of Darcy's law is regained.

By summing u_w and u_o given in Eqs. (3.20) and (3.21), and using the notation introduced in Eqs. (3.25) - (3.27), the total flux can be expressed as:

$$u_T = u_w + u_o = -\hat{\lambda}_T \frac{\partial p_w}{\partial x} - \hat{\lambda}_o \frac{\partial p_c}{\partial x} \tag{3.29}$$

The water pressure gradient can be expressed as

$$\frac{\partial p_w}{\partial x} = -\frac{1}{\hat{\lambda}_T} u_T - (1 - \hat{f}_w) \frac{\partial p_c}{\partial x}, \tag{3.30}$$

where the generalized fractional flow function for water is

$$\hat{f}_w = \frac{\hat{\lambda}_w}{\hat{\lambda}_T}. \tag{3.31}$$

Inserting Eq. (3.30) into Eqs. (3.20) and (3.21), along with the notation in Eqs.

(3.25) - (3.27), the following is obtained:

$$u_w = u_T \hat{f}_w + W\frac{\partial p_c}{\partial x}, \qquad u_o = u_T \hat{f}_o - W\frac{\partial p_c}{\partial x}, \tag{3.32}$$

with definitions:

$$\hat{f_w} = \frac{\hat{\lambda_w}}{\hat{\lambda_T}} = \frac{{S_w}^2 R_o + S_w R}{{S_w}^2 R_o + {S_o}^2 R_w + R}, \tag{3.33}$$

$$W(S_w) = \hat{f_w}\hat{\lambda_o} - \hat{\lambda}_{ow} = \frac{{S_w}^2 {S_o}^2 \phi_e}{{S_w}^2 R_o + {S_o}^2 R_w + R}. \tag{3.34}$$

If the water flux from Eq. (3.32) is inserted into the conservation equation for water, (3.3), we get:

$$\frac{\partial(\phi s_w)}{\partial t} = -\frac{\partial(u_T \hat{f_w})}{\partial x} - \frac{\partial}{\partial x}(W\frac{\partial p_c}{\partial x}). \tag{3.35}$$

For comparison, the equation takes the following form when a conventional Darcy model is used:

$$\frac{\partial(\phi s_w)}{\partial t} = -\frac{\partial(u_T f_w)}{\partial x} - \frac{\partial}{\partial x}(f_w \lambda_o \frac{\partial p_c}{\partial x}). \tag{3.36}$$

The key difference is the extra term $-\hat{\lambda}_{ow}$ that is included in W for the generalized model. Consequently, the generalized model has a built in capability of accounting for the impact of viscous coupling when the flow setting changes from co- to counter-current.

3.4 Specification of interaction terms.

Still, specification of the interaction terms R and $R_i (i = w, o)$ is needed to obtain explicit analytical expressions for the generalized phase mobilities. It should be clear that the solid-fluid interaction terms R_i have to obey the relationship $R_i \propto \mu_i \phi / k$ in order to be consistent with conventional (Darcy) modeling of fluid flow in porous media. The following relations for the interaction terms were included in the generalized model to capture the interaction between fluids flowing in a porous medium (Standnes et al., 2017; Standnes and Andersen, 2017; Qiao et al., 2018):

$$R_w = I_w {S_w}^\alpha \frac{\mu_w}{k}\phi_e, \tag{3.37}$$

$$R_o = I_o {S_w}^\beta \frac{\mu_w}{k}\phi_e, \tag{3.38}$$

$$R = IS_w S_o \frac{\mu_w \mu_o}{k} \phi_e. \tag{3.39}$$

Here, α and β are dimensionless exponents, the terms I_w and I_o are dimensionless coefficients that characterize the magnitude of solid-fluid interaction (friction), while I is a coefficient with units of $(\mathrm{Pa} \cdot \mathrm{s})^{-1}$, characterizing the magnitude of fluid-fluid coupling.

3.5 Generalized relative permeabilities.

3.5.1 Co-current flow.

If we assume a co-current flow regime which is typical during standard coreflooding experiments, a direct link between the generalized and conventional model can be shown, assuming capillary end effects (Rapoport and Leas, 1953; Andersen et al., 2017b) can be ignored. During coreflooding both phases are injected in the same direction with the same pressure gradient, thus yielding:

$$u_w = -\hat{\lambda}_w \frac{\partial p}{\partial x} = -(\hat{\lambda}_{ww} + \hat{\lambda}_{ow}) \frac{\partial p}{\partial x}, \tag{3.40}$$

$$u_o = -\hat{\lambda}_o \frac{\partial p}{\partial x} = -(\hat{\lambda}_{ow} + \hat{\lambda}_{oo}) \frac{\partial p}{\partial x} \tag{3.41}$$

The generalized mobilities $\hat{\lambda}_w$ and $\hat{\lambda}_o$ then represent mobilities that would be measured in a co-current relative permeability measurement. Note that the proportionality factor between u_i and $\partial p_i / \partial x$ should be $-kk_{ri}/\mu_i$, where $(i = w, o)$. Thus, from these mobilities we can construct generalized relative permeabilities expressed in terms of interaction term parameters:

$$\hat{k}_{rw}^{co} = \frac{\mu_w}{k} \hat{\lambda}_w = \frac{\mu_w}{k} (\hat{\lambda}_{ww} + \hat{\lambda}_{ow}) = \frac{S_w S_o^{\beta-1} I_o + S_w \mu_w I}{S_w^{\alpha-1} S_o^{\beta-1} I_o I_w + I(S_w^{\alpha} \mu_w I_w + S_o^{\beta} \mu_o I_o)}, \tag{3.42}$$

$$\hat{k}_{ro}^{co} = \frac{\mu_o}{k} \hat{\lambda}_o = \frac{\mu_o}{k} (\hat{\lambda}_{oo} + \hat{\lambda}_{ow}) = \frac{S_o S_w^{\alpha-1} I_w + S_o \mu_o I}{S_w^{\alpha-1} S_o^{\beta-1} I_o I_w + I(S_w^{\alpha} \mu_w I_w + S_o^{\beta} \mu_o I_o)}. \tag{3.43}$$

It is evident that the generalized relative permeabilities are not only functions of saturations, but also depend on fluid viscosities when $I > 0$. Viscosity dependence has been suggested previously by several authors (Yuster, 1951; Odeh, 1959; Lefebvre du Prey, 1973; Nejad et al., 2011). The resulting relative permeability endpoints are

$$\hat{k}_{rw}^{co}(S_w = 0) = 0, \qquad \hat{k}_{rw}^{co}(S_w = 1) = \frac{1}{I_w}, \tag{3.44}$$

$$\hat{k}_{ro}^{co}(S_w = 0) = \frac{1}{I_o}, \qquad \hat{k}_{ro}^{co}(S_w = 1) = 0. \tag{3.45}$$

Further, if the fluid-fluid interaction parameter I is zero, the relative permeabilities simplify to Corey-type expressions:

$$\hat{k}_{rw}^{co}(I = 0) = \frac{S_w^{2-\alpha}}{I_w}, \tag{3.46}$$

$$\hat{k}_{ro}^{co}(I = 0) = \frac{S_o^{2-\beta}}{I_o}, \tag{3.47}$$

where α and β are related to the Corey exponents n_w and n_o by:

$$\alpha = 2 - n_w, \qquad \beta = 2 - n_o. \tag{3.48}$$

Andersen et al. (2019) and Qiao et al. (2018) showed that the generalized model is able to account for variation in flow mode, by matching both co-current and counter-current experiments using only generalized co-current relative permeabilities. They matched the co-current relative permeabilities and capillary pressure curves reported by Bourbiaux and Kalaydjian (1990), and were able to reproduce oil recovery for both co-current and counter-current SI. Fig. 3.3 shows how the numerical solution of the generalized model was able to capture the delay seen in the counter-current experiment.

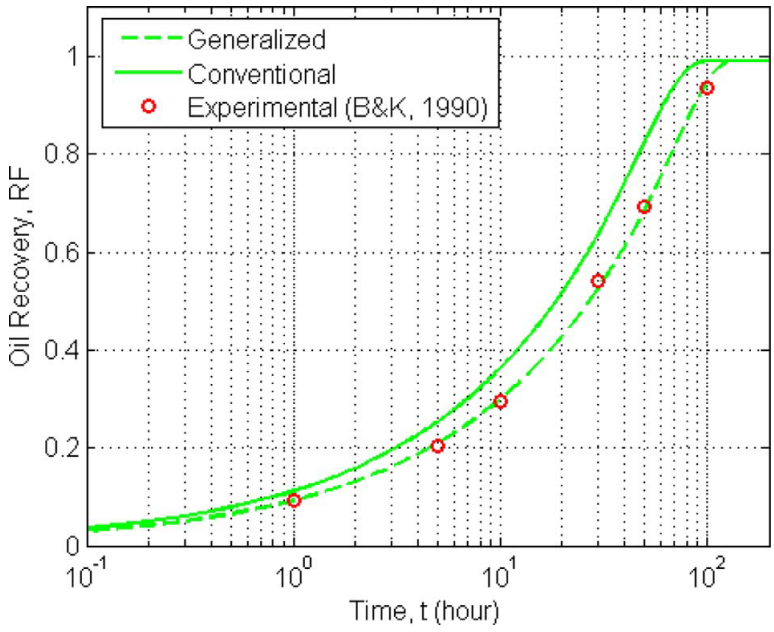

Figure 3.3: Comparison of numerical solutions of the generalized and conventional model with the experimental work (Bourbiaux and Kalaydjian, 1990) for the counter-current SI case (experiment GVB-3 in the original paper). From Qiao et al. (2018).

3.5.2 Counter-current flow.

When the flow mode is changed to purely counter-current, due to conservation of volume, we have fluxes of equal magnitude, but with opposite directions:

$$u_w = -u_o. \tag{3.49}$$

In this section, eq. (3.49) is used to derive generalized mobilities and relative permeabilities for counter-current flow.

The fluxes can be expressed using generalized mobilities as in (3.18) and (3.19), and we obtain:

$$-\hat{\lambda}_{ww}\frac{\partial p_w}{\partial x} - \hat{\lambda}_{ow}\frac{\partial p_o}{\partial x} = \hat{\lambda}_{ow}\frac{\partial p_w}{\partial x} + \hat{\lambda}_{oo}\frac{\partial p_o}{\partial x}. \tag{3.50}$$

The pressure gradients are separated:

$$-\hat{\lambda}_{oo}\frac{\partial p_o}{\partial x} - \hat{\lambda}_{ow}\frac{\partial p_o}{\partial x} = \hat{\lambda}_{ow}\frac{\partial p_w}{\partial x} + \hat{\lambda}_{ww}\frac{\partial p_w}{\partial x}. \tag{3.51}$$

Next, we express the pressure gradients relative to each other:

$$\frac{\partial p_o}{\partial x} = -\frac{(\hat{\lambda}_{ow} + \hat{\lambda}_{ww})}{(\hat{\lambda}_{oo} + \hat{\lambda}_{ow})}\frac{\partial p_w}{\partial x}, \tag{3.52}$$

$$\frac{\partial p_w}{\partial x} = -\frac{(\hat{\lambda}_{oo} + \hat{\lambda}_{ow})}{(\hat{\lambda}_{ow} + \hat{\lambda}_{ww})}\frac{\partial p_o}{\partial x} \tag{3.53}$$

The pressure gradients can now be inserted back into the flux relations. For brevity, this is only shown here for the water flux, since the procedure is the same for the oil flux. The water flux is given by:

$$u_w = -\hat{\lambda}_{ww}\frac{\partial p_w}{\partial x} - \hat{\lambda}_{ow}\frac{\partial p_o}{\partial x} \tag{3.54}$$

The oil pressure gradient is replaced using eq. (3.52):

$$u_w = -\hat{\lambda}_{ww}\frac{\partial p_w}{\partial x} - \hat{\lambda}_{ow}\Big(-\frac{(\hat{\lambda}_{ow} + \hat{\lambda}_{ww})}{(\hat{\lambda}_{oo} + \hat{\lambda}_{ow})}\frac{\partial p_w}{\partial x}\Big) \tag{3.55}$$

After some algebraic manipulation, we obtain the following expression for the water

flux, now only expressed using the water pressure gradient:

$$u_w = -(\hat{\lambda}_{ww} + \hat{\lambda}_{ow})\Big[\frac{\hat{\lambda}_{ww}}{(\hat{\lambda}_{ww} + \hat{\lambda}_{ow})} - \frac{\hat{\lambda}_{ow}}{(\hat{\lambda}_{oo} + \hat{\lambda}_{ow})}\Big]\frac{\partial p_w}{\partial x} \tag{3.56}$$

The corresponding oil flux in terms of the oil pressure gradient is:

$$u_o = -(\hat{\lambda}_{ow} + \hat{\lambda}_{oo})\Big[\frac{\hat{\lambda}_{oo}}{(\hat{\lambda}_{ow} + \hat{\lambda}_{oo})} - \frac{\hat{\lambda}_{ow}}{(\hat{\lambda}_{ow} + \hat{\lambda}_{ww})}\Big]\frac{\partial p_o}{\partial x} \tag{3.57}$$

If we now compare equations (3.56) and (3.57) to the co-current versions (3.40) and (3.41), we see that they differ by the factor enclosed in square brackets. Further, we again note that the proportionality factor between u_i and $\partial p_i/\partial x$ should be $-kk_{ri}/\mu_i$, where $(i = w, o)$. This is used to obtain the following generalized relative permeabilities for purely counter-current flow:

$$\hat{k}_{rw}^{cou} = \frac{\mu_w}{k}(\hat{\lambda}_{ww} + \hat{\lambda}_{ow})\Big[\frac{\hat{\lambda}_{ww}}{(\hat{\lambda}_{ww} + \hat{\lambda}_{ow})} - \frac{\hat{\lambda}_{ow}}{(\hat{\lambda}_{oo} + \hat{\lambda}_{ow})}\Big], \tag{3.58}$$

$$\hat{k}_{ro}^{cou} = \frac{\mu_o}{k}(\hat{\lambda}_{ow} + \hat{\lambda}_{oo})\Big[\frac{\hat{\lambda}_{oo}}{(\hat{\lambda}_{ow} + \hat{\lambda}_{oo})} - \frac{\hat{\lambda}_{ow}}{(\hat{\lambda}_{ow} + \hat{\lambda}_{ww})}\Big]. \tag{3.59}$$

The key point here is that the counter current relative permeabilities are actually the co-current relative permeabilities from eqs. (3.42) and (3.43), multiplied by the factors in square brackets. The superscript *cou* is used for identification. Thus, we can write:

$$\hat{k}_{rw}^{cou} = \hat{k}_{rw}^{co}\Big[\frac{\hat{\lambda}_{ww}}{(\hat{\lambda}_{ww} + \hat{\lambda}_{ow})} - \frac{\hat{\lambda}_{ow}}{(\hat{\lambda}_{oo} + \hat{\lambda}_{ow})}\Big], \tag{3.60}$$

$$\hat{k}_{ro}^{cou} = \hat{k}_{ro}^{co}\Big[\frac{\hat{\lambda}_{oo}}{(\hat{\lambda}_{ow} + \hat{\lambda}_{oo})} - \frac{\hat{\lambda}_{ow}}{(\hat{\lambda}_{ow} + \hat{\lambda}_{ww})}\Big], \tag{3.61}$$

where the square bracketed factors will be referred to as counter-current factors. Finally, we apply the definitions of the mobility terms from eqs. (3.22) - (3.24) and the definitions for the interaction terms R_w, R_o and R from eqs. (3.37) - (3.39). We now get generalized relative permeabilities for counter-current flow, expressed using interaction term parameters α, β, I_w, I_o, I , μ_w and μ_o. The full expressions, after

simplification, are as follows:

$$\hat{k}_{rw}^{cou} = \frac{S_w S_o^{\beta-1} I_o + S_w \mu_w I}{S_w^{\alpha-1} S_o^{\beta-1} I_o I_w + I(S_w^{\alpha} \mu_w I_w + S_o^{\beta} \mu_o I_o)} \cdot \Big[\frac{I_o S_o^{\beta-1} + I S_w \mu_w}{I_o S_o^{\beta-1} + I \mu_w} - \frac{I S_w \mu_o}{I_w S_w^{\alpha-1} + I \mu_o}\Big], \quad (3.62)$$

$$\hat{k}_{ro}^{cou} = \frac{S_o S_w^{\alpha-1} I_w + S_o \mu_o I}{S_w^{\alpha-1} S_o^{\beta-1} I_o I_w + I(S_w^{\alpha} \mu_w I_w + S_o^{\beta} \mu_o I_o)} \cdot \Big[\frac{I_w S_w^{\alpha-1} + I S_o \mu_o}{I_w S_w^{\alpha-1} + I \mu_o} - \frac{I S_o \mu_w}{I_o S_o^{\beta-1} + I \mu_w}\Big]. \quad (3.63)$$

3.5.3 Counter-current end points

For $I > 0$, the following relative permeability end points are obtained for water:

$$\begin{aligned} &\hat{k}_{rw}^{cou}(S_w = 0) = 0, \\ &\hat{k}_{rw}^{cou}(S_w = 1) = \frac{1}{I_w}\Big[\frac{I_w}{I_w + I\mu_o}\Big] = \frac{1}{I_w + I\mu_o}. \end{aligned} \quad (3.64)$$

Similarly for oil, we get:

$$\begin{aligned} &\hat{k}_{ro}^{cou}(S_w = 0) = \frac{1}{I_o}\Big[\frac{I_o}{I_o + I\mu_w}\Big] = \frac{1}{I_o + I\mu_w}, \\ &\hat{k}_{ro}^{cou}(S_w = 1) = 0. \end{aligned} \quad (3.65)$$

Thus, when the fluid-fluid interaction term is non-zero, the counter-current end-points will be lower than the co-current end points due to the extra terms in the denominators of Eqs. (3.64) and (3.65). For the water relative permeability, the magnitude of this difference depends on the values of the solid-fluid interaction term, I_w, the fluid-fluid interaction term I and the viscosity of the oil phase, μ_o. Similarly, for the oil relative permeability, the magnitude of the difference depends on the values of the solid-fluid interaction term, I_o, the fluid-fluid interaction term I and the viscosity of the water phase, μ_w. For $I = 0$, the counter-current factors become unity for all saturations, and there is no difference between $\hat{k}_{ri}^{co}$ and $\hat{k}_{ri}^{cou}$ $(i = w, o)$. The behaviour of the relative permeability curves for different input parameters is studied further in the first part of the results section. The generalized

relative permeabilities will be implemented in the analytical solution for counter-current SI and compared to numerical solutions of both the conventional model and the generalized model.

3.5.4 Relation between co- and counter-current generalized relative permeabilities

From Eqs. (3.62) and (3.63), it is seen that the factors enclosed in square brackets relate the counter-current relative permeability to the co-current relative permeability. For convenience and clarity, the relations can be rewritten as:

$$C_w = \frac{\hat{k}_{rw}^{cou}}{\hat{k}_{rw}^{co}} = \Big[\frac{I_o S_o^{\beta-1} + I S_w \mu_w}{I_o S_o^{\beta-1} + I\mu_w} - \frac{I S_w \mu_o}{I_w S_w^{\alpha-1} + I\mu_o}\Big], \tag{3.66}$$

$$C_o = \frac{\hat{k}_{ro}^{cou}}{\hat{k}_{ro}^{co}} = \Big[\frac{I_w S_w^{\alpha-1} + I S_o \mu_o}{I_w S_w^{\alpha-1} + I\mu_o} - \frac{I S_o \mu_w}{I_o S_o^{\beta-1} + I\mu_w}\Big], \tag{3.67}$$

where C_w and C_o have been introduced to denote the counter-current factors for water and oil, respectively.

Chapter 4

Analytical solutions

4.1 Solution for 1-D, co-current flow (Buckley-Leverett).

The analytical solution for a two-phase, 1-D, co-current flow scenario was first presented by Buckley and Leverett (1942). It's validity is conditioned on a set of assumptions concerning the porous media and fluids involved. The assumptions are as follows:

- Horizontal, homogeneous reservoir of length L and cross sectional area A_c.
- Incompressible and immiscible fluids, oil and water.
- Incompressible reservoir with porosity ϕ and permeability k.
- No capillary pressure. Flow driven by external pressure. This also implies that the pressure gradient is equal in both phases.
- Reservoir is initially filled with oil ($S_o(x, t = 0) = 1$).
- Water injected with rate Q at one end, production at the other end (pure co-current flow).
- Impact of gravity can be ignored. This assumption holds if Q is sufficiently high.

Incompressibility of the reservoir and fluids implies that the total flow rate will be controlled by and equal to Q at any point along the reservoir. Darcy velocity is defined as $u = Q/A_c$. The extension of Darcy's law to two-phase flow is applied. Darcy velocities or fluid fluxes for oil and water are given by

$$u_o = -\frac{kk_{ro}}{\mu_o}\frac{\partial p}{\partial x}, \tag{4.1}$$

$$u_w = -\frac{kk_{rw}}{\mu_w}\frac{\partial p}{\partial x}, \tag{4.2}$$

where k_{ro} and k_{rw} are relative permeabilities for oil and water respectively, and μ_o and μ_w are oil and water viscosities. Viscosities are assumed constant, while relative permeabilities are functions of fluid saturations S_o and S_w. The total flux u_T follows from the constraint $S_o + S_w = 1$:

$$u_T = u_o + u_w = \frac{Q}{A_c}. \tag{4.3}$$

4.1.1 Deriving the Buckley-Leverett equation.

The fluxes u_w and u_o above can be inserted into the conservation equations for water and oil, resulting in the following:

$$\frac{\partial}{\partial x}(\frac{kk_{rw}}{\mu_w}\frac{\partial p}{\partial x}) = \phi\frac{\partial S_w}{\partial t}, \tag{4.4}$$

$$\frac{\partial}{\partial x}(\frac{kk_{ro}}{\mu_o}\frac{\partial p}{\partial x}) = \phi\frac{\partial S_o}{\partial t}. \tag{4.5}$$

Water and oil mobilities are defined by:

$$\lambda_w = \frac{kk_{rw}}{\mu_w}, \tag{4.6}$$

$$\lambda_o = \frac{kk_{ro}}{\mu_o}. \tag{4.7}$$

Rewriting the mass balance equations using mobilities gives:

$$\frac{\partial}{\partial x}(\lambda_w\frac{\partial p}{\partial x}) = \phi\frac{\partial S_w}{\partial t}, \tag{4.8}$$

$$\frac{\partial}{\partial x}(\lambda_o\frac{\partial p}{\partial x}) = \phi\frac{\partial S_o}{\partial t}. \tag{4.9}$$

Equations (4.8) and (4.9) are added, resulting in:

$$\frac{\partial}{\partial x}[(\lambda_w + \lambda_o)\frac{\partial p}{\partial x}] = \phi(\frac{\partial S_w}{\partial t} + \frac{\partial S_o}{\partial t}). \tag{4.10}$$

The time derivatives on the right hand side cancel out due to the saturation constraint $S_w + S_o = 1$. Further, the mobilities can be expressed using total mobility $\lambda_T = \lambda_w + \lambda_o$. Thus, (4.10) becomes:

$$\frac{\partial}{\partial x}(\lambda_T \frac{\partial p}{\partial x}) = 0 \tag{4.11}$$

The total flux $u_T = Q/A_c$ can now be expressed in terms of the total mobility:

$$u_T = u_w + u_o = -(\lambda_w + \lambda_o)\frac{\partial p}{\partial x} = -\lambda_T \frac{\partial p}{\partial x} \tag{4.12}$$

From the above, an expression for the pressure gradient is obtained:

$$\frac{\partial p}{\partial x} = -\frac{u_T}{\lambda_T}. \tag{4.13}$$

This is used to eliminate the pressure term in the mass balance equation for water. Combining (4.8) and (4.13) yields:

$$\frac{\partial}{\partial x}(-u_T \frac{\lambda_w}{\lambda_T}) = \phi \frac{\partial S_w}{\partial t}. \tag{4.14}$$

Since u_T is constant due to constant injection rate Q, and introducing the water fractional flow function f, Eq. (4.14) can be rewritten as the Buckley-Leverett equation

$$\phi \frac{\partial S_w}{\partial t} + u_T \frac{\partial f}{\partial x} = 0, \tag{4.15}$$

where f is defined by

$$f = \frac{\lambda_w}{\lambda_T} = \frac{\frac{kk_{rw}}{\mu_w}}{\frac{kk_{rw}}{\mu_w} + \frac{kk_{ro}}{\mu_o}}. \tag{4.16}$$

Alternatively, dividing through by kk_{rw}/μ_w, f can be expressed as

$$f = \frac{1}{1 + \frac{k_{ro}\mu_w}{k_{rw}\mu_o}} = (1 + \frac{k_{ro}\mu_w}{k_{rw}\mu_o})^{-1}. \tag{4.17}$$

4.1.2 Frontal advance equation

Since

$$S_w = S_w(x, t), \tag{4.18}$$

a change in saturation can be expressed as

$$dS_w = \frac{\partial S_w}{\partial x}dx + \frac{\partial S_w}{\partial t}dt. \tag{4.19}$$

The idea of the Buckley-Leverett solution is to follow a plane of constant saturation as it travels along the reservoir. Expressing constant saturation as

$$\frac{\partial S_w}{\partial x}dx + \frac{\partial S_w}{\partial t}dt = 0 \tag{4.20}$$

and substituting this into the BL equation (4.15) yields:

$$\frac{dx}{dt} = \frac{u_T}{\phi}\frac{df}{dS_w} \tag{4.21}$$

Integration in time and considering the fractional flow derivative at a specific saturation gives an expression for the position of that saturation:

$$x_{Sw} = \frac{u_T t}{\phi}(\frac{df}{dS_w})_{Sw} \tag{4.22}$$

where x_{Sw} is the position of the saturation plane and df/dS_w is the speed at which the plane of constant saturation moves along the reservoir.

4.1.3 Dimensionless variables

For convenience we can introduce dimensionless position $x_D = x/L$ and dimensionless time $t_D = u_T t/\phi L$. The dimensionless time is equal to the number of injected pore volumes. Eq. (4.22) on dimensionless form then becomes:

$$x_D = (\frac{df}{dS_w})t_D. \tag{4.23}$$

From here on, the subscript D is dropped, but note that dimensionless position and time is still used. This implies that $0 \leq x \leq 1$ and $t \geq 0$.

4.1.4 Physically correct saturation profile

We denote dimensionless time time corresponding to real time t by T. Application of the frontal advance equation and plotting water saturation against distance gives an impossible, unphysical solution. For the illustration of this phenomenon, simple Corey-type expressions have been used to generate relative permeability curves for

computation of the fractional flow function. For this simple example we use the values given in Table 4.1 and consider the case where T=0.4.

Table 4.1: Input for simple Corey-type relative permeability curves.

Parameter	Value
$k_{rw,max}$	1
$k_{ro,max}$	1
n_w	2
n_o	2
μ_w/μ_o	0.5

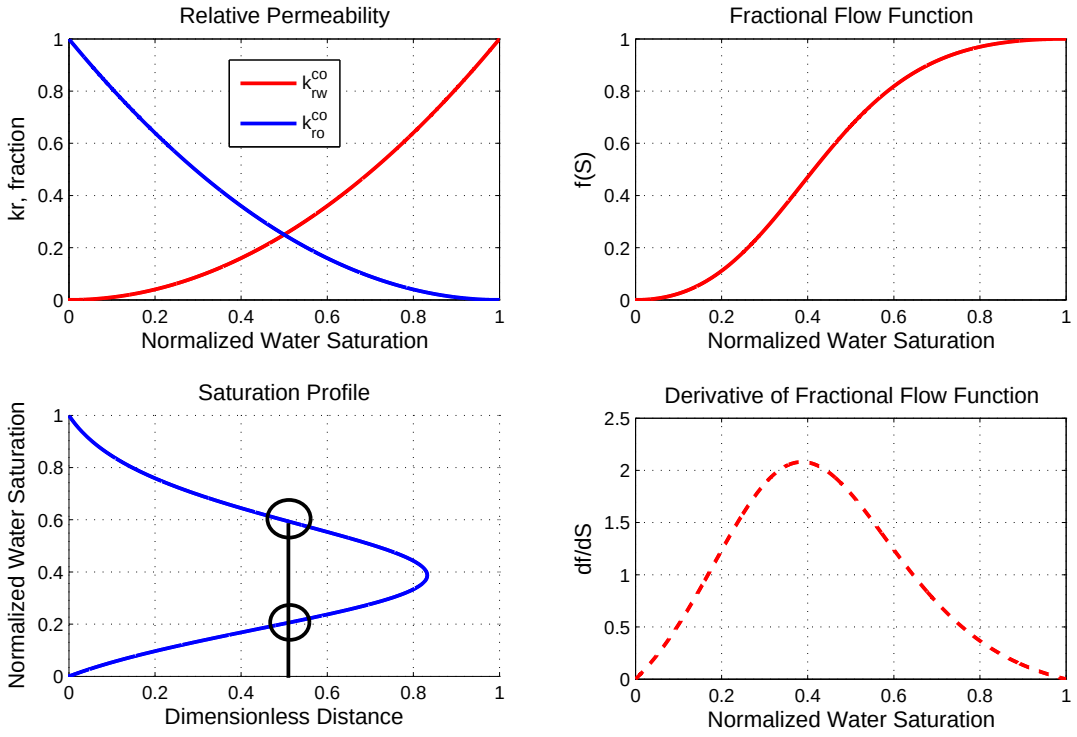

Figure 4.1: Top: Corey-type relative permeabilities and resulting fractional flow function. Bottom: Unphysical saturation profile at T=0.4 and the derivative of the fractional flow function.

Fig. 4.1 shows how simply moving every saturation along according to $x_{Sw} = f'(S_w)T$, results in an impossible saturation profile. Each position along the x-axis corresponds to two different water saturations. This is a consequence of the S-shaped fractional flow curve and the resulting shape of the derivative $f'(S)$. To obtain a physically correct solution, a shock front is introduced, and an area balancing argument is applied. Referring to Fig. 4.2, due to mass conservation, the area of the unphysical profile (A1) has to be equal to the area of the profile where a shock front has been introduced (A2). The areas can be calculated by integrating the

saturation profile over the saturation range:

$$A1 = \int_0^1 f'(S)TdS = T, \tag{4.24}$$

$$A2 = S_f x_f + \int_{S_f}^1 f'(S)TdS = S_f f'(S_f)T + (1 - f(S_f))T, \tag{4.25}$$

where S_f is the shock front saturation and x_f is the position of the shock. By equating the areas, we can obtain the following relation:

$$f'(S_f) = \frac{f(S_f)}{S_f}. \tag{4.26}$$

The front saturation can now be found from defining a function

$$g(S) = f'(S_f)S_f - f(S_f) \tag{4.27}$$

and finding where $g(S) = 0$. The front saturation can also be found graphically

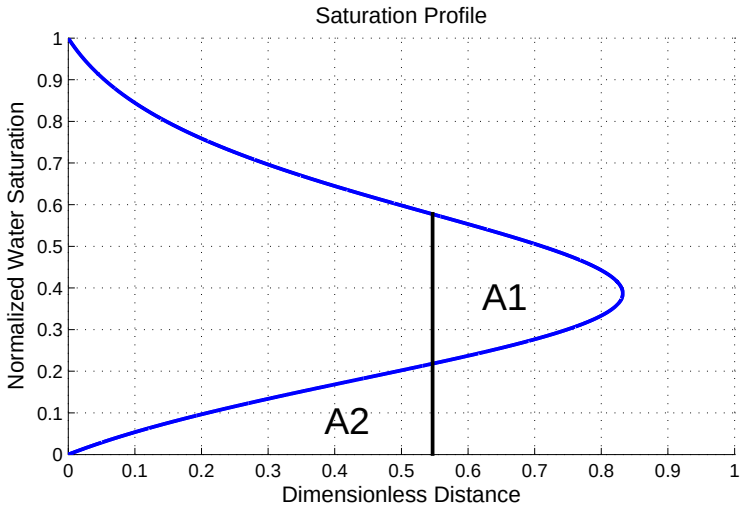

Figure 4.2: Area balancing to determine shock front saturation.

from the tangent of the fractional flow curve that passes through (0,0). Similarly, the speed of any saturation $S > S_f$ can be found from the derivative of the fractional flow curve at that specific water saturation.

The position of the front at any time is found by multiplying the speed of the front with the time that has elapsed:

$$x_f = f'(S_f)T, \tag{4.28}$$

and the profile behind the front is found similarly by using the speed $f'(S)$:

$$x = f'(S)T. \tag{4.29}$$

Thus the correct saturation profile is finally obtained and shown in Fig. 4.3. Lastly,

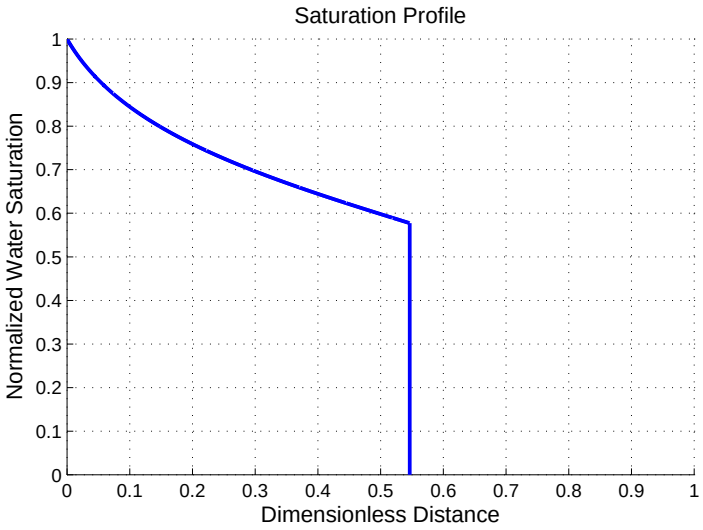

Figure 4.3: Correct saturation profile for T=0.4.

we can find the breakthrough time, T_{bt}, when the front reaches the end of the reservoir at $x = 1$ from:

$$T_{bt} = \frac{1}{f'(S_f)}. \tag{4.30}$$

4.2 Solution for counter-current spontaneous imbibition

While the Buckley-Leverett solution for forced imbibition has been known for a long time, and is well established, a general analytical solution for SI has been missing up until fairly recently. The Lucas-Washburn equation (Lucas, 1918; Washburn, 1921) predicted that the process of spontaneous imbibition scales with $\sqrt{t}$ in time. Despite this early insight and substantial research efforts into SI and scaling groups spanning over 90 years, the exact nature of SI time scaling was not sufficiently understood until Schmid and Geiger (2012, 2013) published a general scaling group based on previous work by McWhorter and Sunada (1990). In the meantime, several analytical solutions and scaling groups were presented. They all came with additional assumptions that meant lack of generality and limited applicability. Schmid and Geiger (2012) gave a comprehensive overview of non-general solutions and scaling groups with inherent limitations. Examples of limiting assumptions are specific functional forms for relative permeabilities and capillary pressure (Fokas and Yortsos, 1982; Philip, 1960; Chen, 1988; Kashchiev and Firoozabadi, 2003) or piston-like displacement (Li et al., 2003).

4.2.1 Relevant equations

We now consider 1D, horizontal flow of oil and water in a homogeneous porous medium with capillary pressure included and no gravity term. The previously derived conservation equation for water is repeated for convenience:

$$\phi \frac{\partial s_w}{\partial t} + \frac{\partial u_w}{\partial x} = 0. \tag{4.31}$$

The water flux, u_w, can be written (Dake, 1983; Helmig, 1997):

$$u_w = f_w u_T + \lambda_o f_w \frac{dp_c}{ds_w} \frac{\partial s_w}{\partial x}, \tag{4.32}$$

where f_w is the same fractional flow function that was used in the Buckley-Leverett solution:

$$f_w = (1 + \frac{k_{ro}\mu_w}{k_{rw}\mu_o})^{-1} \tag{4.33}$$

For the counter-current case, we have $u_w = -u_o$ which leads to $u_T = 0$. Hence, the first term in eq. (4.32) is zero for this case. Combination of (4.31) and (4.32) then yields:

$$\phi \frac{\partial s_w}{\partial t} = \frac{\partial}{\partial x}\Big[D(s_w)\frac{\partial s_w}{\partial x}\Big], \tag{4.34}$$

where the capillary diffusion coefficient $D(s_w)$ has been introduced. It has units of length squared over time and is defined as follows:

$$D(s_w) = -\lambda_o f_w \frac{dp_c}{ds_w}. \tag{4.35}$$

The capillary diffusion coefficient describes the capillary-hydraulic properties of the porous media-fluid system, and thus controls the flow that results from the capillary pressure gradient. Mathematically rigorous derivations of solutions to eq. (4.34) can be found in the works of McWhorter and Sunada (1990) and Schmid et al. (2011). It is outside the scope of this work, where the focus is on implementing the analytical solutions for comparison against numerical solutions.

In their original paper, McWhorter and Sunada (1990) derived solutions for co- and counter-current displacement of non-wetting and wetting phases. They also included solutions for radial flow. In the following, the main results that are relevant for the case considered in this thesis (i.e. purely counter-current displacement of a non-wetting phase) are presented, and the procedure for solving the equations is outlined.

4.2.2 Solution in integral form

For our horizontal reservoir with one end open to imbibition we consider the following boundary and initial conditions:

$$s_w(x = 0, t) = s_0, \tag{4.36}$$

$$s_w(\infty, t) = s_i, \tag{4.37}$$

$$s_w(x, 0) = s_i, \tag{4.38}$$

where the use of ∞ signifies that the solution was derived for an infinite medium, and thus for a finite medium the solution will only be valid until it reaches the closed end boundary. The saturation condition at the inlet, s_0, represents the maximum water saturation that can be reached during spontaneous imbibition. In our case this will be equal to $1 - s_{or}$, since for a strongly water-wet material, we assume a positive capillary pressure for the whole saturation range where oil is mobile. The initial water saturation, s_i will be equal to the irreducible or residual water saturation, s_{wr}. McWhorter and Sunada (1990) made no limiting assumptions regarding the physics or on the capillary-hydraulic properties of the system that are contained in $D(s_w)$. Instead they specified an extra boundary condition that describes the inflow at the open end as

$$u_0 = u_w(x = 0, t) = At^{-1/2}, \tag{4.39}$$

where A is referred to as the inflow parameter, and for a given system is a constant that describes the system's ability to imbibe water. In short, the solution was found

through a variable transformation of the form $\eta = xt^{-1/2}$. This made it possible to rewrite the problem as a non-linear first order differential equation, which is solvable using an iterative procedure (March et al., 2016).

The inflow parameter A can then be found from

$$A^2 = \frac{\phi}{2} \int_{s_i}^{s_0} \frac{(s_w - s_i)D(s_w)}{F(s_w)} ds_w, \tag{4.40}$$

and is related to the total volume of water imbibed , Q_w, by

$$Q_w(t) = \int_0^t u_w(0,t)dt = 2At^{1/2}. \tag{4.41}$$

$F(s_w)$ represents a fractional flow function for counter-current spontaneous imbibition and can be regarded as the capillary counterpart to $f_w(s_w)$ (Schmid and Geiger, 2013; March et al., 2016). It is defined as:

$$F(x,t) = \frac{u_w(x,t)}{u_0(t)}, \tag{4.42}$$

meaning it describes the ratio of water flux at some x, t to the water flux at the inlet, u_0 (i.e. the maximum water flux). $F(s_w)$ can be obtained by solving the implicit integral equation

$$F(s_w) = 1 - \Big[\int_{s_w}^{s_0} \frac{(\beta - s_w)D(\beta)}{F(\beta)} d\beta \Big] \cdot \Big[\int_{s_i}^{s_0} \frac{(s_w - s_i)D(s_w)}{F(s_w)} ds_w \Big]^{-1}, \tag{4.43}$$

where the integration variable β represents water saturations and has only been used to avoid confusion with s_w in the first integral. When $F(s_w)$ is known, its derivative can be found from

$$F'(s_w) = \Big[\int_{s_w}^{s_0} \frac{D(\beta)}{F(\beta)} d\beta \Big] \cdot \Big[\int_{s_i}^{s_0} \frac{(s_w - s_i)D(s_w)}{F(s_w)} ds_w \Big]^{-1}, \tag{4.44}$$

or alternatively, since $F(s_w)$ is known, the derivative can be found by numerical differentiation. The solution to Eq. (4.34) with the specified boundary conditions (Eqs. (4.36) - (4.38)) can then be written in terms of the inflow parameter, A, and the derivative of $F(s_w)$, together with the condition on $u_w(0,t)$ (McWhorter and Sunada, 1990):

$$x(s_w, t) = \frac{2A}{\phi} F'(s_w) t^{1/2} = \frac{Q_w(t)}{\phi} F'(s_w). \tag{4.45}$$

This can be used to construct saturation profiles and to calculate oil recovery, since the volume of produced oil must be equal to the total amount of imbibed water in the purely counter-current process considered here.

4.2.3 Computing $F(s_w)$ iteratively

Since $F(s_w)$ given by Eq. (4.43) depends on itself, it has to be computed using an iterative procedure as outlined in this section (McWhorter and Sunada, 1990; Nooruddin and Blunt, 2016). The first step is to calculate the capillary diffusion coefficient, $D(s_w)$ from known relative permeabilities and capillary pressure curves, as it is part of the implicit integrals to be solved. The iterative computations are then initiated by assuming a starting value of $F(s_w) = 1$ for all values of s_w. Using this first guess, the integrals can be computed, and an updated $F(s_w)$ is found. The updated $F(s_w)$ can then be inserted into the integrals to compute the next iteration. The iterative process continues until the difference between the updated and previous value satisfies a specified tolerance condition for convergence.

4.2.4 Time t*, when the solution becomes invalid

As mentioned previously, the analytical solution is only valid as long as the saturation front has not reached the closed end boundary. The time when the front reaches the end of the core is denoted t^* and is obtained by setting $x(s_w, t) = L$ in Eq. (4.45), where L is the length of the core/reservoir in question (March et al., 2016):

$$t^* = \left(\frac{L\phi}{2AF'(s_{wr})}\right)^2. \tag{4.46}$$

Chapter 5

Results and discussion

5.1 Generalized mobility constraints

Under the assumption made for counter-current flow, $u_w = -u_o$, we get the following phase fluxes:

$$u_w = -(\hat{\lambda}_{ww} + \hat{\lambda}_{ow})\Big[\frac{\hat{\lambda}_{ww}}{(\hat{\lambda}_{ww} + \hat{\lambda}_{ow})} - \frac{\hat{\lambda}_{ow}}{(\hat{\lambda}_{oo} + \hat{\lambda}_{ow})}\Big]\frac{\partial p_w}{\partial x} \tag{5.1}$$

$$u_o = -(\hat{\lambda}_{oo} + \hat{\lambda}_{ow})\Big[\frac{\hat{\lambda}_{oo}}{(\hat{\lambda}_{ow} + \hat{\lambda}_{oo})} - \frac{\hat{\lambda}_{ow}}{(\hat{\lambda}_{ow} + \hat{\lambda}_{ww})}\Big]\frac{\partial p_o}{\partial x}. \tag{5.2}$$

The counter-current factor (in square brackets) has a maximum value of unity when $\hat{\lambda}_{ow} = 0$, that is when there is no fluid-fluid interaction. It is however not directly apparent if the factor can become negative. This would happen if the second term is larger than the first, and can be expressed as the following inequality (using the water expression):

$$\frac{\hat{\lambda}_{ow}}{(\hat{\lambda}_{oo} + \hat{\lambda}_{ow})} > \frac{\hat{\lambda}_{ww}}{(\hat{\lambda}_{ww} + \hat{\lambda}_{ow})} \tag{5.3}$$

If this inequality holds, it would mean that for some combination of inputs, we would get negative mobilities and therefore negative relative permeabilities. Standnes et al. (2017) found that certain values of the input parameters resulted in negative values for relative permeability. This was particularly the case when I was large and one of the phases had a low saturation, making it sensitive to viscous coupling. While they worked with the same generalized model, the assumption made for counter-current flow was pressure gradients of equal magnitude, but opposite directions. In this work we assume equal, but opposite phase fluxes, a key distinction. Nevertheless, their results motivate the check performed here.

Continuing, we multiply by the denominators and simplify:

$$\hat{\lambda}_{ow}(\hat{\lambda}_{ww} + \hat{\lambda}_{ow}) > \hat{\lambda}_{ww}(\hat{\lambda}_{oo} + \hat{\lambda}_{ow}) \tag{5.4}$$

$$\hat{\lambda}_{ow}\hat{\lambda}_{ww} + \hat{\lambda}_{ow}^2 > \hat{\lambda}_{ww}\hat{\lambda}_{oo} + \hat{\lambda}_{ww}\hat{\lambda}_{ow} \tag{5.5}$$

$$\hat{\lambda}_{ow}^2 > \hat{\lambda}_{ww}\hat{\lambda}_{oo} \tag{5.6}$$

The generalized mobility terms are defined as:

$$\hat{\lambda}_{ww} = \frac{{S_w}^2(R_o + R)}{R_oR_w + R(R_o + R_w)}\phi_e, \tag{5.7}$$

$$\hat{\lambda}_{oo} = \frac{{S_o}^2(R_w + R)}{R_oR_w + R(R_o + R_w)}\phi_e, \tag{5.8}$$

$$\hat{\lambda}_{wo} = \hat{\lambda}_{ow} = \frac{S_wS_oR}{R_oR_w + R(R_o + R_w)}\phi_e. \tag{5.9}$$

Inserting this into the inequality:

$$(\frac{S_wS_oR}{R_oR_w + R(R_o + R_w)}\phi_e)^2 > \frac{{S_w}^2(R_o + R)}{R_oR_w + R(R_o + R_w)}\phi_e\frac{{S_o}^2(R_w + R)}{R_oR_w + R(R_o + R_w)}\phi_e \tag{5.10}$$

This simplifies greatly to:

$$R^2 > (R_o + R)(R_w + R) \tag{5.11}$$

$$R^2 > R_oR_w + R_oR + R_wR + R^2 \tag{5.12}$$

$$0 > R_oR_w + R_oR + R_wR \tag{5.13}$$

Since all the terms on the right hand side of (5.13) are defined to be larger than or equal to zero, the inequality does not hold. Thus, the conclusion is that the counter-current scaling factor can not be negative under the assumption for counter-current flow that is applied in this work.

5.2 Base case for input parameters

The numerical solutions were proven by Qiao et al. (2018) by matching the experimental results of Bourbiaux and Kalaydjian (1990). To establish a base case for comparisons, the input parameters from Qiao et al. (2018) have been applied, hence we can be assured that the base input parameters are in fact realistic values. The only exception is the parameters used to generate the capillary pressure curve. This was changed due to quicker computation of the numerical solutions. For this reason, and due to the fact that gravity is ignored in this work, the results are not directly comparable to their previous work, which also included gravity.

The parameters for the base case are given in table 5.1, and the capillary pressure curves are plotted in Fig. 5.1 for comparison. Unless otherwise is indicated, these input parameters are assumed.

Table 5.1: Input parameters for the base case considered for counter-current SI.

Parameter	Value	Parameter	Value
L	0.29 m	I_w	23.26
ϕ	0.233	I_o	2.15
s_{wr}	0.4	I	3500 $(\text{Pa} \cdot \text{s})^{-1}$
s_{or}	0.425	α	-0.2
μ_w	1.2 mPa $\cdot$ s	β	1.5
μ_o	1.5 mPa $\cdot$ s	a_1	0.56
k	118 mD	a_2	0.66
σ	15.8 mN/m	k_1	1.25
		k_2	0.08
		c	0.55

Co-current and counter-current relative permeabilities for the base case are plotted in Fig. 5.2. There is a significant difference between the curves. Both end points have been reduced, as suggested by Eqs. (3.64) and (3.65). For a better illustration of the differences, the counter-current factors have been plotted in Fig. 5.3. Interestingly, and not obvious from Eqs. (3.62) and (3.63) , the water and oil factors are equal. Consequently, for a given saturation, the co-current relative permeabilities for both oil and water are scaled down by the same factor when we assume counter-current flow. For the base case inputs, the factors plot approximately on a straight line, with a higher reduction in permeability (i.e. lower factor) at low water saturations.

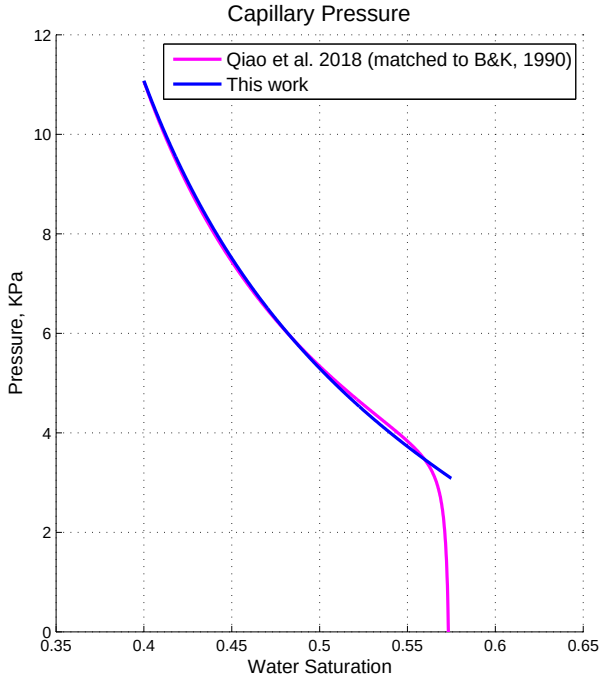

Figure 5.1: Comparison of capillary pressure curves. Blue: This work. Magenta: Qiao et al. (2018), matched to measurements from Bourbiaux and Kalaydjian (1990).

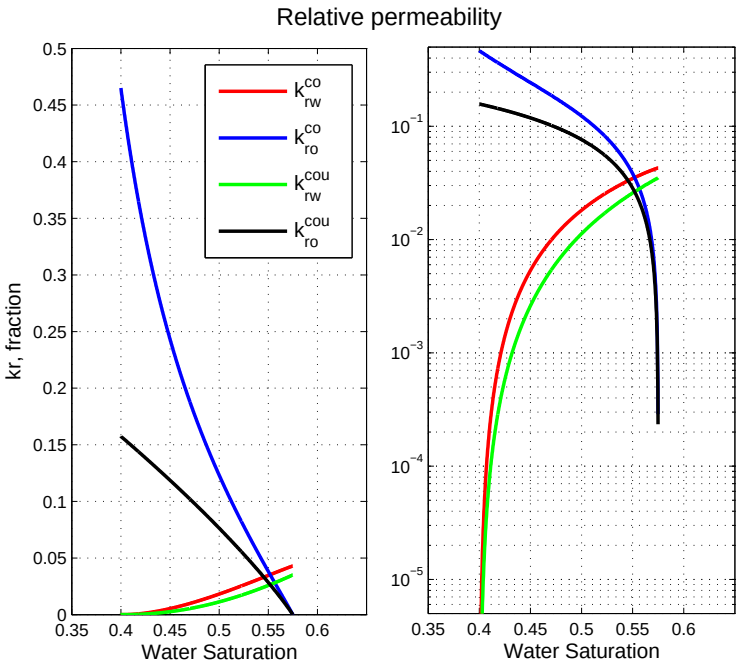

Figure 5.2: Comparison of generalized co-current and counter-current relative permeability curves for the base case. Input parameters are given in table 5.1. Left: linear scale, right: log-scale.

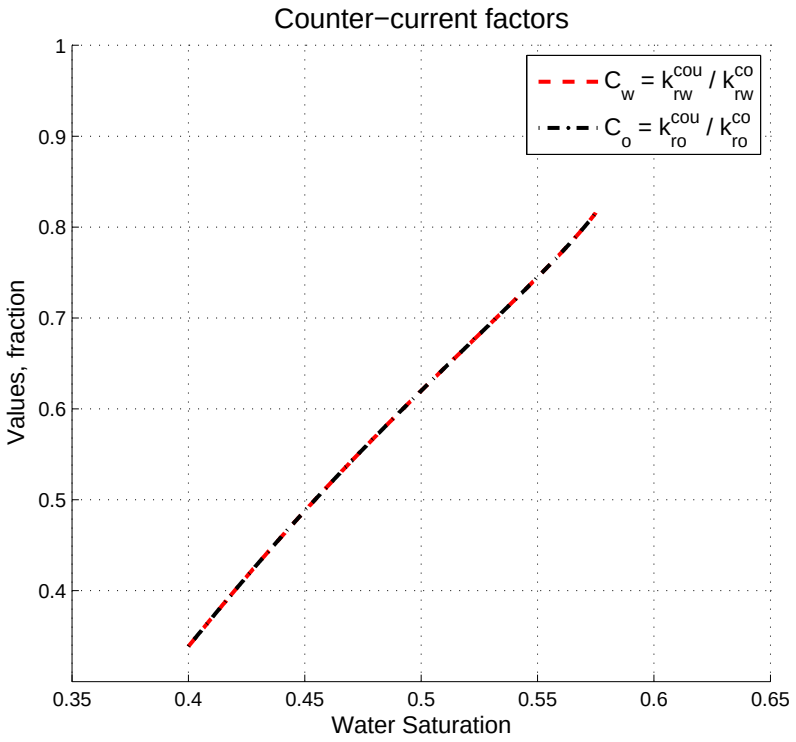

Figure 5.3: Counter-current factors C_w and C_o, as given by Eqs. (3.66) and (3.67) for the base case.

5.3 Effect of input parameters on relative permeabilities

This section focuses specifically on the newly derived generalized relative permeability curves. Input parameters are varied to investigate the role of each parameter on the resulting curves. We focus on the fluid-fluid interaction parameter I that controls viscous coupling, as well as the fluid viscosities μ_w and μ_o, as these have a direct physical interpretation.

5.3.1 Fluid-fluid interaction parameter

The fluid-fluid interaction parameter I controls the magnitude of viscous coupling, and increasing it should in theory result in a larger difference between co- and counter-current relative permeabilities. This is due to the idea that viscous coupling is more important when the fluids flow in opposite directions. From Fig. 5.4 we can see that this is exactly what happens. The co-current oil curve (blue) changes curvature and is decreased as I increases. The co-current water curve (red), however, increases with increased I. We can interpret this as follows: In a co-current flow, increasing I would lead to a deceleration of oil and an acceleration of the water. We also note that for the co-current curves there is no change in end points, which is in line with the equations. Plots of the counter-current factors reveal that as I takes on

larger values, the difference between co- and counter-current relative permeabilities is indeed increased, and notably more significantly at lower water saturations.

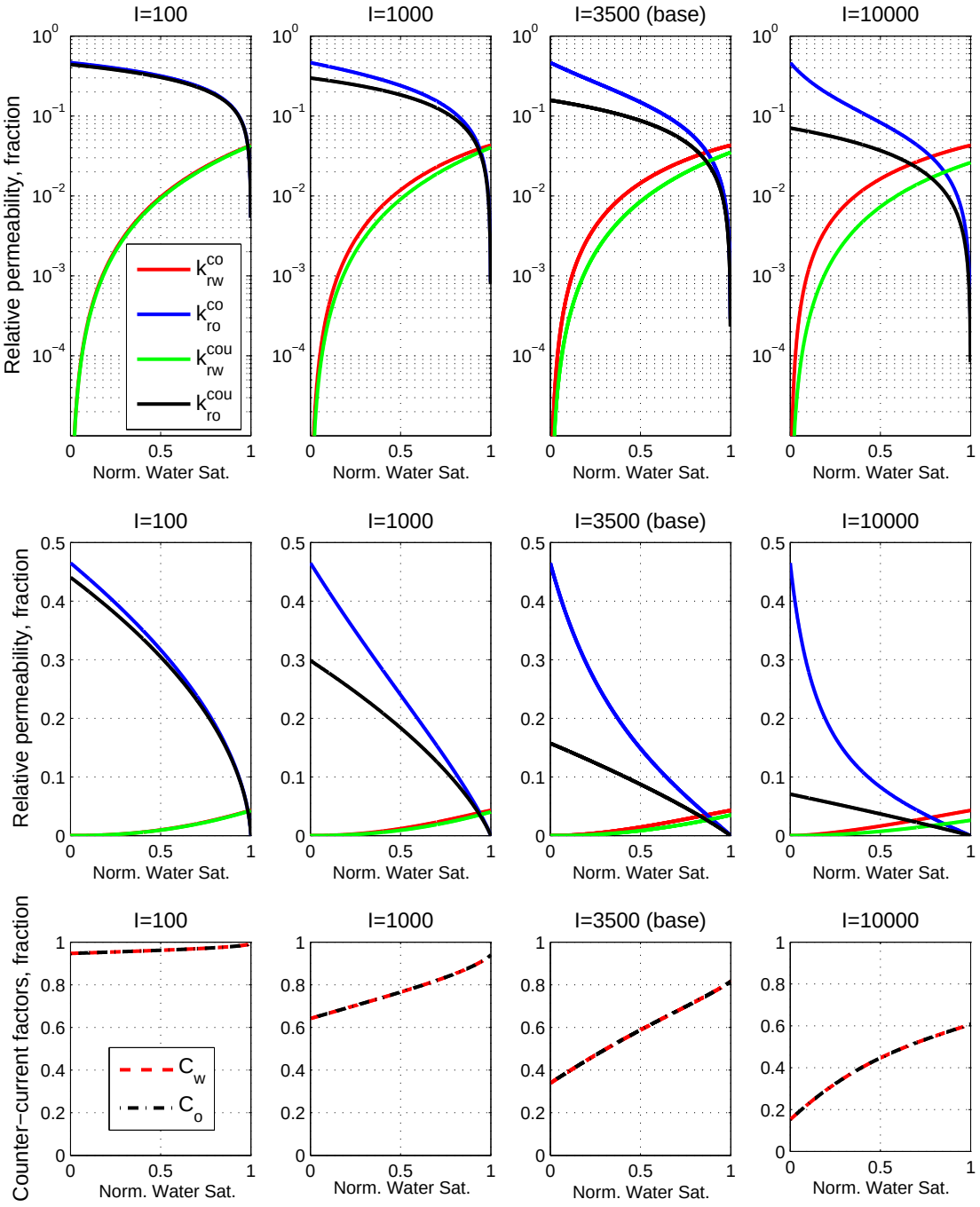

Figure 5.4: Top row: Relative permeabilities for $I = 100$, $I = 1000$, $I = 3500$ (base case) and $I = 10000$. I has units of $(\text{Pa} \cdot \text{s})^{-1}$. Middle row: Same as top, linear scale. Bottom row: Corresponding counter-current factors.

5.3.2 Water viscosity

Fig. 5.5 shows the effect of increasing water viscosity by factors of 2, 10 and 100 relative to the base case. The following trends are observed for larger values of μ_w: Co-current oil relative permeability is decreased significantly. Co-current water relative permeability is increased at low water saturation. The differences between co- and counter-current relative permeabilities are again more significant at lower water saturations (i.e. the counter-current factors are lower). The end point for the counter-current oil curve decreases with increasing water viscosity, in line with Eq. (3.65), while there is no effect on the end point for water. There is, however, still a difference between the co-current and counter-current end points for water due to a non-zero I.

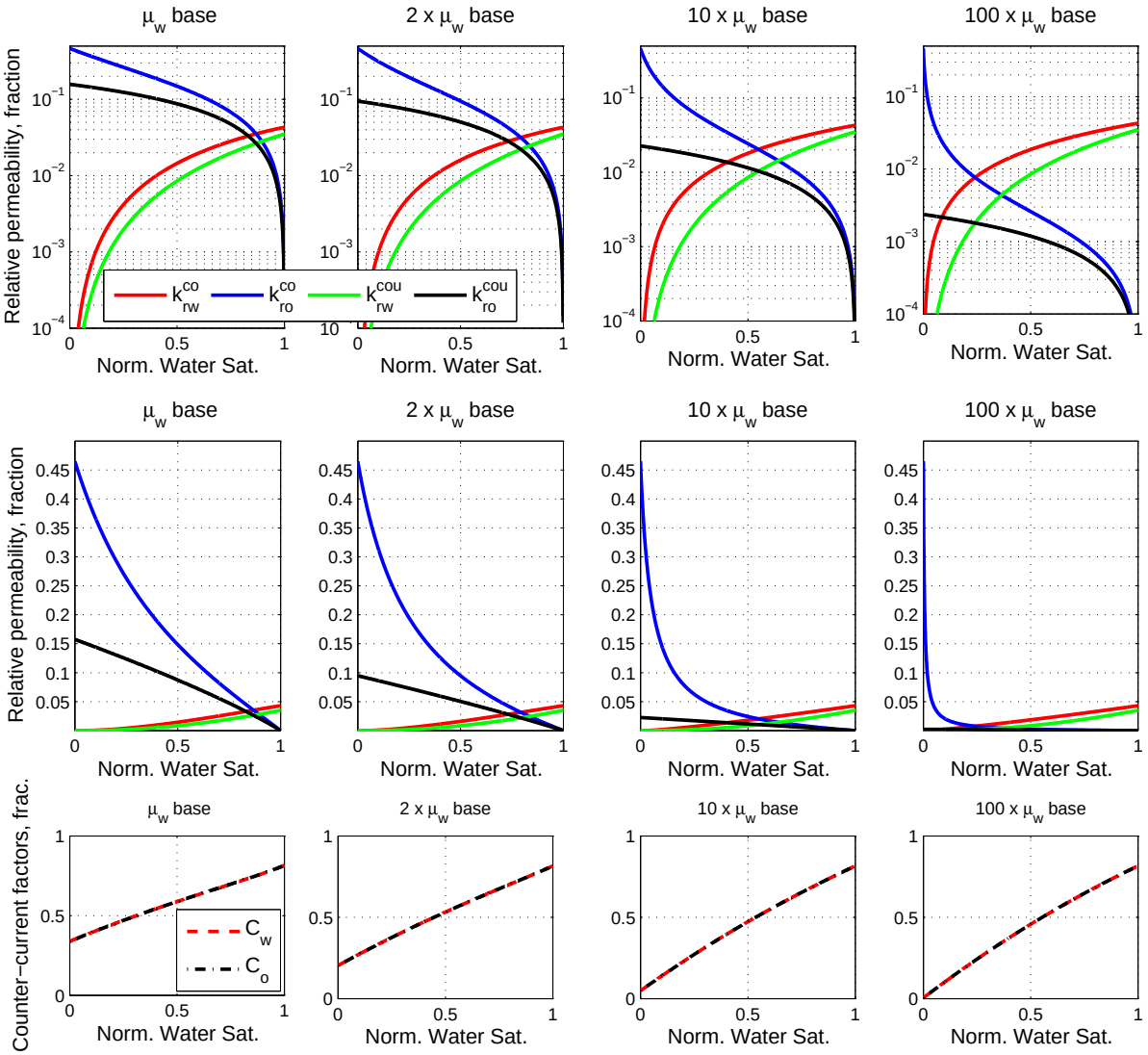

Figure 5.5: Comparison of relative permeabilities and counter-current factors for increasing water viscosity. From left to right: μ_w from base case (used as reference), 2xμ_w, 10xμ_w and 100x μ_w.

5.3.3 Oil viscosity

We use the same approach as for water viscosity to study the effect of changing oil viscosity. Relative permeability curves that result from increasing oil viscosity by factors of 2, 10 and 100 relative to the base case are shown in Fig. 5.6.

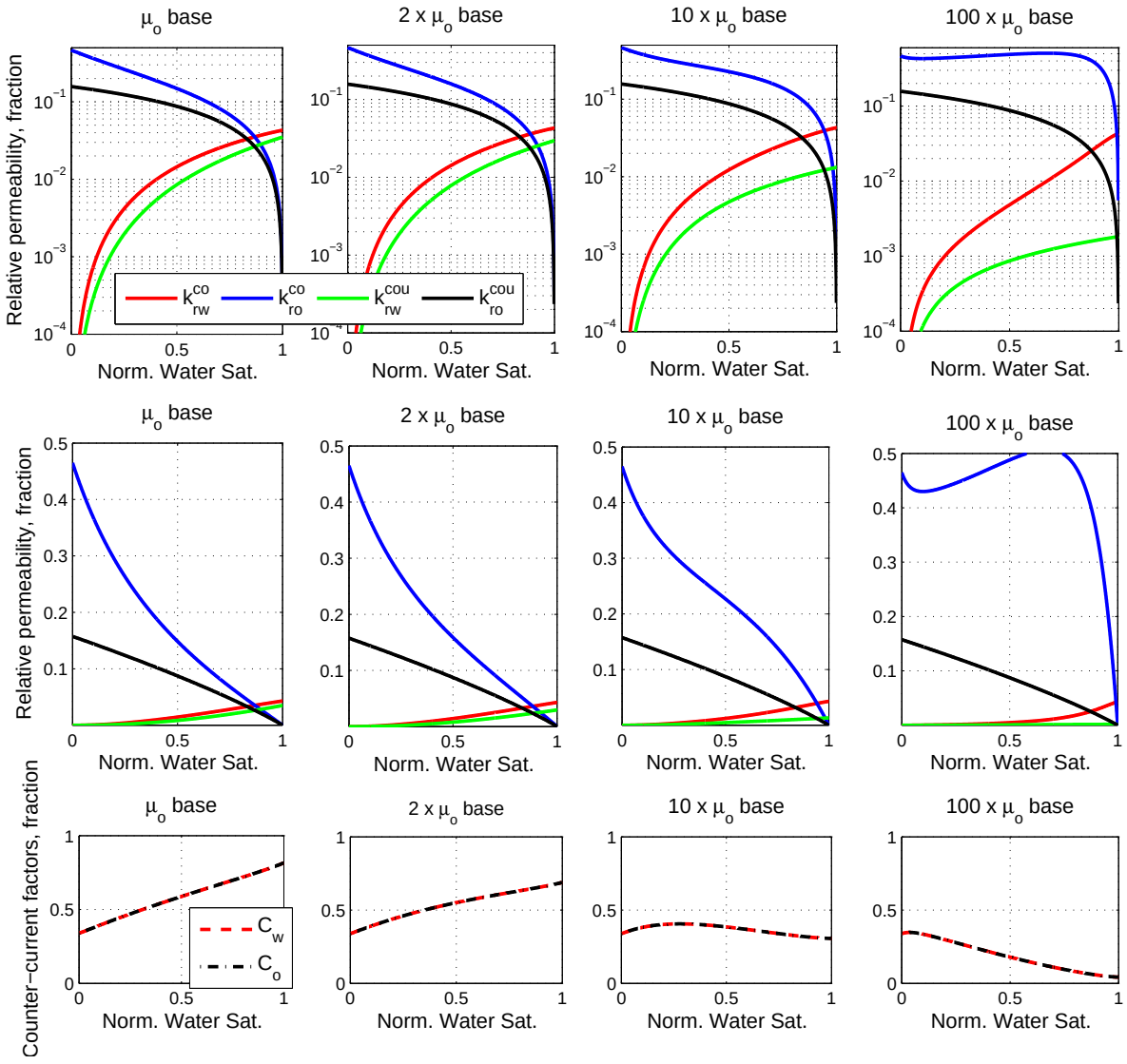

Figure 5.6: Comparison of relative permeabilities and counter-current factors for increasing oil viscosity. From left to right: μ_o from base case (used as reference), 2xμ_o, 10xμ_o and 100x μ_o.

For the co-current oil relative permeability, we see an increase across the whole saturation range as oil viscosity increases. At the extreme case of 100 times the base viscosity, we actually observe values that are slightly higher than the end point value for oil. Similar results, although not as extreme were seen in the work of Andersen et al. (2019). They used a lower value for the fluid-fluid term (I=2500) and the saturation exponents were $\alpha = 0.0, \beta = 1.0$, which could explain the difference. As with any correlation, there could be other sets of parameters that would produce

good match to the original experimental results.

The behaviour seen for the co-current oil curve does not match results by Wang et al. (2006), who found that both oil and water relative permeability shifted to lower values as oil viscosity increased. It is possible that certain values of the saturation exponents α and β should be avoided. In particular, the combination of $\beta = 1.5$ with high oil viscosity produces a questionable looking co-current oil curve. This corresponds to a Corey-exponent of $n_o = 0.5$, whereas a typical value would be $n_o > 1$. While relative permeability curves showing inflection points have been observed (Muskat et al., 1937; Anderson, 1987; Honarpour et al., 1996), the behaviour seen here seems rather extreme, and is possibly a result of a too large value for the saturation exponent, β. This has not been explored in further detail in this work, as the focus has been on the fluid-fluid interaction term and the fluid viscosities.

The counter-current oil curve looks to be relatively unaffected by changes in oil viscosity. The co-current water curve shows a decrease as oil viscosity increases, as does the counter-current curve. A new behaviour is observed for the counter-current factors, where we now see progressively lower factors at high water saturations as oil viscosity is increased.

Further, it is interesting to note that the counter-current factors C_w and C_o, which relate the co- and counter-current curves, are not constants, but vary with water saturation for a given set of input parameters (if $I \neq 0$). Thus, the expressions derived here indicate a more complex relationship between co- and counter-current relative permeabilities than what was suggested by Bourbiaux and Kalaydjian (1990). As mentioned earlier, they suggested decreasing the oil relative permeabilities by 60% of the co-current values, water relative permeabilities by 45% of their co-current values, or both by around 30%. All of these approaches are essentially just scaling the co-current curves by a constant.

Viscosity-dependent end points for the counter-current curves is in line with the results obtained by Standnes et al. (2017), however their expressions also included the residual saturation of the opposite phase in a non-trivial way. Their expressions also led to viscosity dependent end points for co-current relative permeabilities, whereas in this work, the co-current end points are only dependent on the solid-fluid interaction terms I_w and I_o. Variation in co-current end point values with viscosity were also observed experimentally by Nejad et al. (2011) and Odeh (1959).

The general observation is that when viscous coupling is included (i.e. $I \neq 0$), counter-current relative permeabilities are always lower than the corresponding co-current values for a given set of input parameters. Hence, we have agreement with the results of previous researchers who found that fluids experience greater flow resistance, thus lower mobilities when travelling in opposite directions (Babchin et al., 1998; Bentsen and Manai, 1992; Bourbiaux and Kalaydjian, 1990; Dullien and Dong, 1996).

5.4 Forced imbibition (Buckley-Leverett)

5.4.1 Results with base case parameters

In this section, the effect of viscous coupling and variations in fluid viscosities are studied for the simple Buckley-Leverett case concerning forced imbibition. The assumptions for the system are those given previously in the description of the solution (Section 4.1). Since this is a purely co-current flow setting, the generalized co-current relative permeabilities are used. The base case (Table 5.1) then represents a system where the end point mobility ratio is much lower than unity, typically referred to as favourable. Hence, the water will push the oil in front of it in a piston-like manner, with a sharp saturation jump from $S_w = 0$ in the unswept region to $S_w = 1$ behind the front. As can be seen from Fig. 5.7, there is no S-shape on the fractional flow function, and as a consequence df/dS is increasing over the whole saturation range. The saturation profile is shown for $T = 0.5$, corresponding to injection of 0.5 PV (pore volumes) and a recovery factor, $RF = 0.5$.

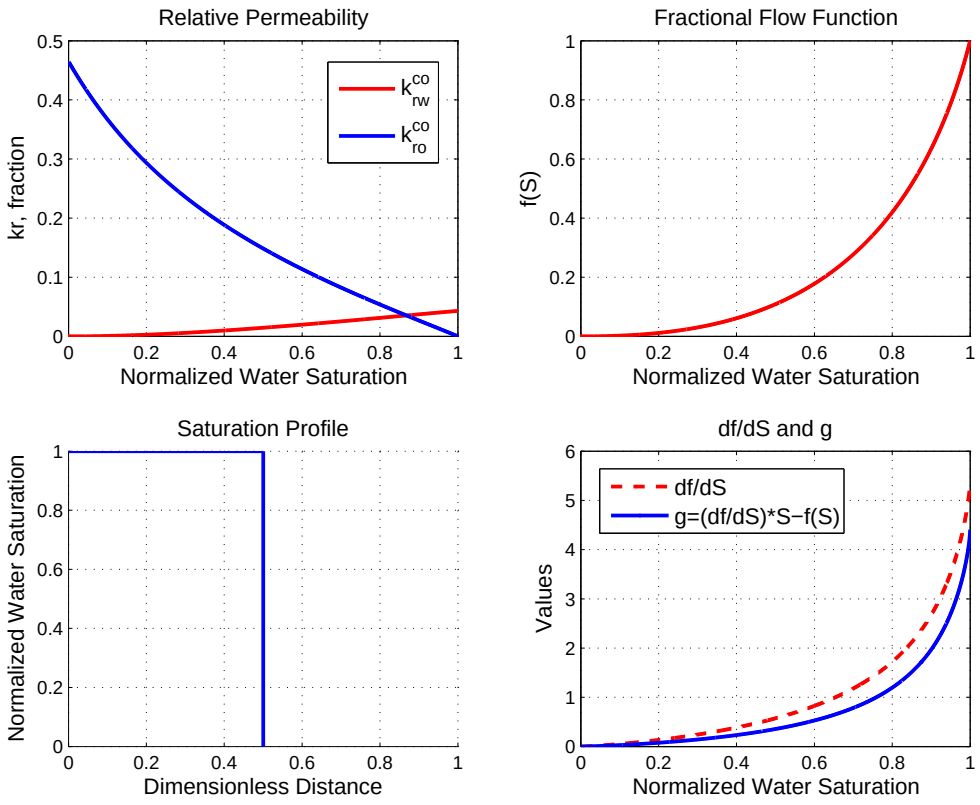

Figure 5.7: Top left: Generalized co-current relative permeabilities for the base case input parameters. Top right: The corresponding fractional flow function. Bottom left: Saturation profile at T=0.5 (0.5 PV's injected). Bottom right: The derivative of the fractional flow function, df/dS and g, both increasing over the whole saturation range.

In order to see differences in saturation profiles and oil recovery, we need to consider cases that do not result in piston-like displacements. If we were dealing with simple Corey-type relative permeability expressions, where there is no viscosity dependence, this could be achieved through increasing oil viscosity. A typical result for such a case is presented in Fig. 5.8, where parameters listed in table 5.2 were used. Since the fluid-fluid interaction parameter I was set to zero, the relative permeability expressions become Corey-type with water and oil exponents $n_w = n_o = 2$:

$$\hat{k}_{rw}^{co} = \frac{S_w^{2-\alpha}}{I_w}, \quad \hat{k}_{ro}^{co} = \frac{S_o^{2-\beta}}{I_o}. \tag{5.14}$$

Table 5.2: Input parameters for demonstration of standard responses in a BL-case.

Parameter	Value	Multiplication factors
I_w	23.26	-
I_o	2.15	-
I	0	-
α	0	-
β	0	-
μ_w	1.2 mPa $\cdot$ s	-
μ_o	1.5 mPa $\cdot$ s	1, 5, 10, 50

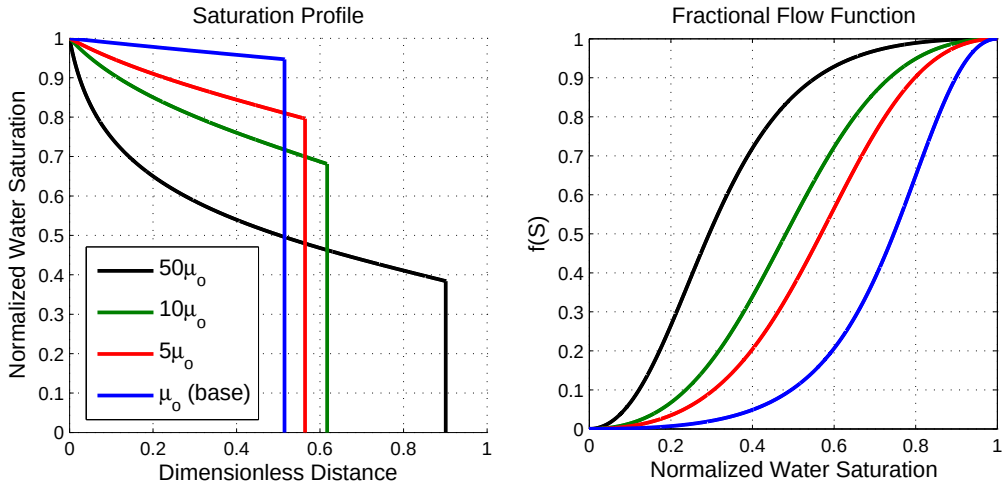

Figure 5.8: Illustration of typical response for increases in oil viscosity from a base of 1.5 mPa $\cdot$ s by factors of 5, 10, 50. Saturation profiles are plotted for the same T=0.5 PV. Input parameters from Table 5.2 have been used.

We see that as oil viscosity increases, the displacement becomes more inefficient, seen as a decrease in the shock front saturation and an advance in the shock front position (earlier breakthrough). This behaviour is standard and expected.

Table 5.3: Input parameters for increased oil viscosity by a factor of 50 from the base case.

Parameter	Value	Multiplication factors
I_w	23.26	-
I_o	2.15	-
I	3500	-
α	-0.2	-
β	1.5	-
μ_w	1.2 mPa $\cdot$ s	-
μ_o	1.5 mPa $\cdot$ s	50

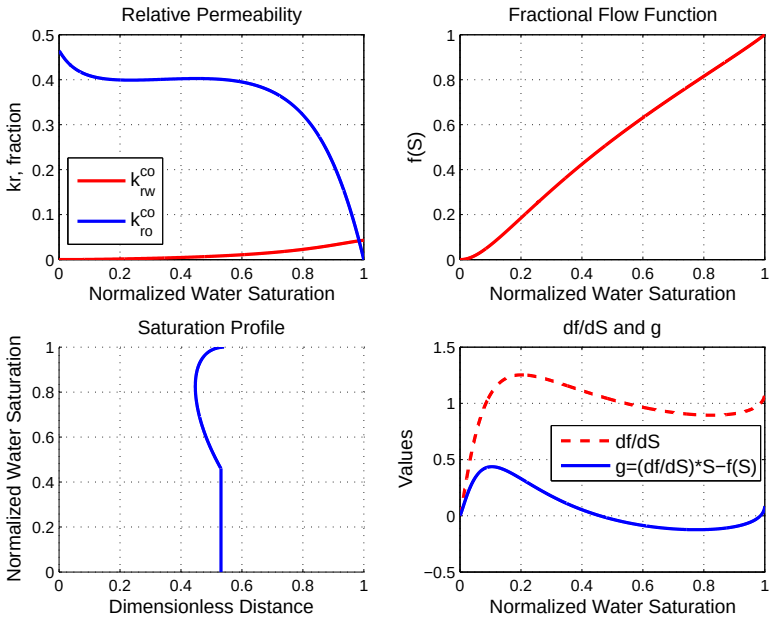

Figure 5.9: Unphysical saturation profile at T=0.5 PV. Result of increasing oil viscosity by a factor of 50 relative to the base case with other parameters unchanged.

However, for the viscosity dependant generalized relative permeabilities we have from the base case, changing the oil viscosity also affects the relative permeability curves. Fig. 5.9 presents the results that are produced when increasing oil viscosity by a factor of 50, relative to the base case. Clearly, the saturation profile is problematic and non-physical. The strange shape of the saturation profile for saturations above the front saturation is caused by the shape of the fractional flow function. This is more visible from the plot of df/dS, where we see that the derivative starts increasing again at approximately $S_w > 0.8$. The root cause is likely the shape of the oil relative permeability curve. Here we again have a case with $\beta = 1.5$ and high oil viscosity producing questionable results. There seems to be two plausible solutions: Either $\beta = 1.5$ is too high and should be avoided during matching, as alluded to in the previous section. Alternatively, the unphysical saturation profile should be modified by constructing a second front behind the shock front using an area

balancing argument. The former option should probably be explored first, however it has not be covered in this work.

Hence, in an effort to obtain results that are interpretable, the oil saturation exponent, β, was changed to zero. For a case where $I = 0$, this corresponds to a more typical Corey exponent of $n_o = 2$.

5.4.2 Results with $\beta = 0$

After lowering the oil saturation exponent β, we get results that appear to be more reasonable. Fig. 5.10 shows the impact of increasing oil viscosity for a case where the fluid-fluid interaction parameter is non-zero. The interpretation is that there should be exchange of momentum between the phases, where the faster moving phase should get slowed down and the slower moving phase should speed up. Hence, we expect to see that water experiences larger flow resistance and shows less tendency to bypass the oil.

Table 5.4: Input parameters for saturation profiles with non-zero I and for increasing oil viscosities.

Parameter	Value	Multiplication factors
I_w	23.26	-
I_o	2.15	-
I	3500	-
α	-0.2	-
β	0	-
μ_w	1.2 mPa $\cdot$ s	-
μ_o	1.5 mPa $\cdot$ s	1, 5, 10, 50

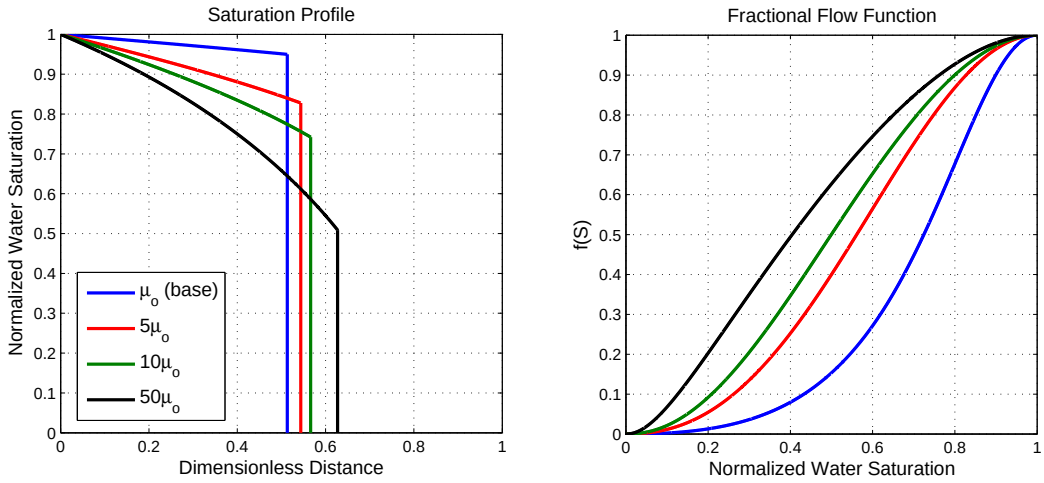

Figure 5.10: Comparison of saturation profiles at T=0.5 PV and fractional flow functions. Result of increasing oil viscosity by factors of 5, 10, 50 with parameters given in Table 5.4.

The saturation profiles presented in Fig. 5.10 are distinctly different from those that resulted from Corey-type relative permeabilities and $I = 0$ (Fig. 5.8). In particular, we notice that the curvature of the profiles behind the shock front is opposite. Thus, when we assume viscous coupling is important (i.e. non-zero I), we get a more efficient displacement with increased shock front saturation and higher average saturation behind the front due to the change in profile curvature. These results are therefore in agreement with the theory of momentum exchange at the fluid-fluid interface.

Increasing the water viscosity will bring us towards a piston-like displacement, in which case there is not much insight to be had. Plots of this has not been included. Instead we can look at what happens if we keep a high oil viscosity while increasing the fluid-fluid interaction parameter. Fig. 5.11 presents results where the oil viscosity was set to 50 times the base case value and I was varied between 0 and 35000. Also here we see that increased viscous coupling leads to a more efficient displacement by increasing the front height and changing the curvature of the profile behind the shock.

Table 5.5: Input parameters for saturation profiles with varying I and high oil viscosity.

Parameter	Value	Multiplication factors
I_w	23.26	-
I_o	2.15	-
I	3500	0, 1, 5, 10
α	-0.2	-
β	0	-
μ_w	1.2 mPa $\cdot$ s	-
μ_o	1.5 mPa $\cdot$ s	50

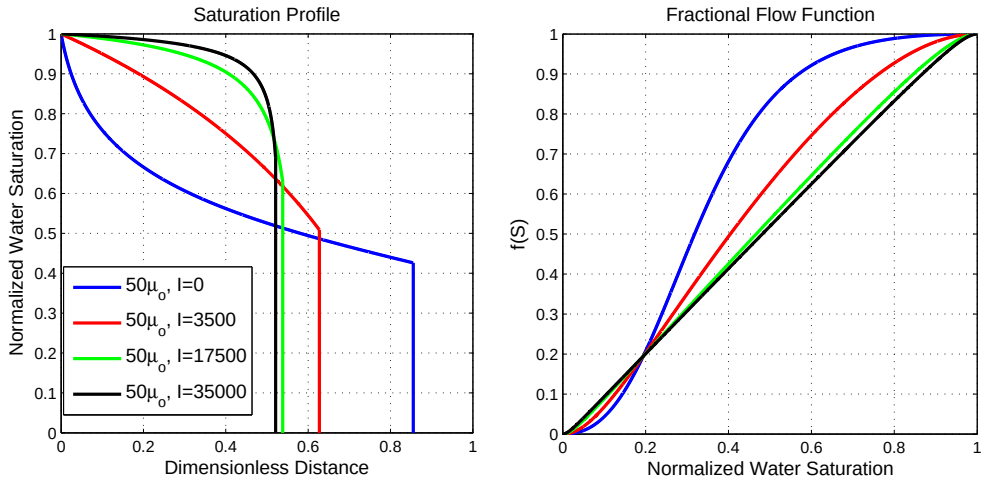

Figure 5.11: Comparison of saturation profiles at T=0.5 PV and fractional flow functions. Result of increasing I at constant, high oil viscosity. Parameters given in Table 5.5.

5.5 Counter-current spontaneous imbibition

In this section analytical solutions for counter-current SI are compared to numerical solutions of the conventional and generalized model.

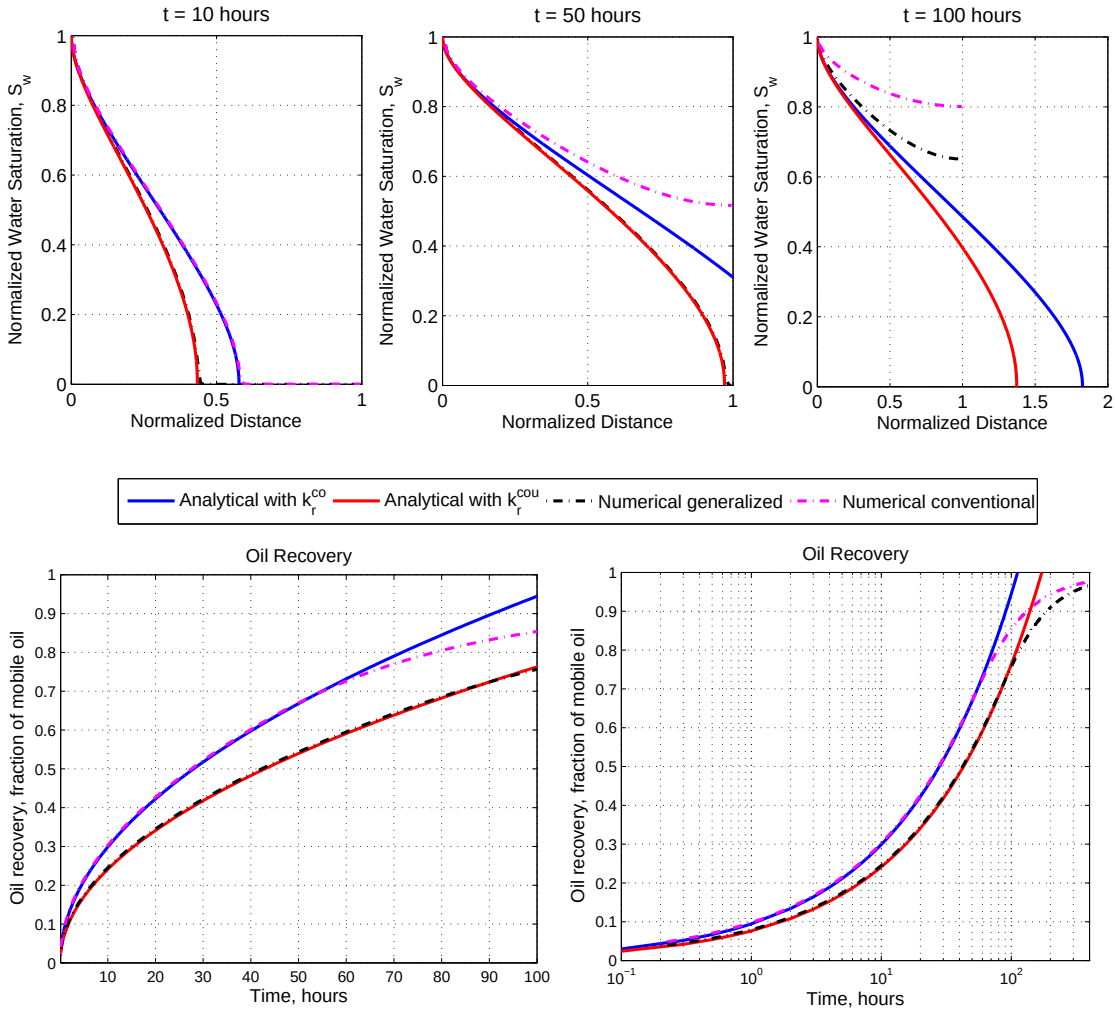

Figure 5.12: Top: Saturation profiles for t=10, 50 and 100 hours for the base case. Note the extended x-axis for t=100 hours to illustrate the difference between analytical and numerical solutions. Bottom: Oil recovery for the four solutions of the base case. Analytical solutions match the numerical solutions in the valid time range.

Fig. 5.12 displays the saturation profiles and oil recovery plots for the four different solutions considered in this work. That is, analytical solutions with co- and counter-current generalized relative permeabilities and numerical solutions of the conventional and generalized model. Excellent matches have been obtained, where the numerical solution of the conventional model matches the analytical solution with co-current relative permeabilities, and the numerical solution of the generalized

model matches the analytical solution with counter-current relative permeabilities. Notice that the x-axis has been extended for t=100 hours to illustrate the difference between the numerical and analytical solutions after the fronts have reached the end of the core. If we look at the saturation profiles at t=50 hours, we see that the analytical solution with co-current relative permeabilities has passed the end of the core and is therefore strictly no longer valid. However, looking at the plot of oil recovery, the solutions seem to match up until approximately 60 hours, where the numerical solution starts dropping off. This will be the same for the analytical solution with counter-current relative permeabilities, but the divergence from the numerical solution will come later due to the imbibition process being slower.

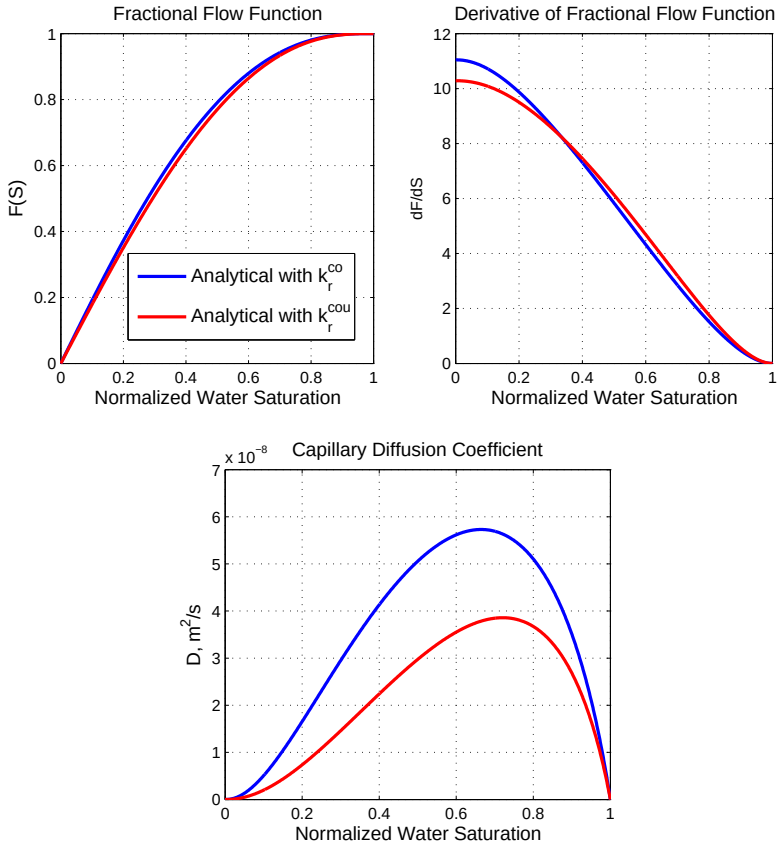

Figure 5.13: Top left: Comparison of fractional flow functions for the analytical solutions with generalized co- and counter-current relative permeabilities. Top right: dF/dS vs. normalized water saturation. Bottom: The capillary diffusion coefficient, D, for both sets of relative permeabilities. Larger values when co-current curves are used indicate higher imbibition rate.

5.5.1 Effect of the fluid-fluid interaction parameter

To investigate the impact of increased coupling, saturation profiles at a time equal to 20 hours have been plotted for increasing values of the fluid-fluid interaction parameter I. The time $t = 20h$ was chosen as both analytical solutions are still valid at this time for the inputs given in the base case (Table 5.1). That is, the normalized position of the saturation front is still less than unity for both cases. Fig. 5.14 shows numerical and analytical saturation profiles for $I = 3500$, $I = 7000$ and $I = 35000$, corresponding to the base case and an increase by factors of 2 and 10, respectively.

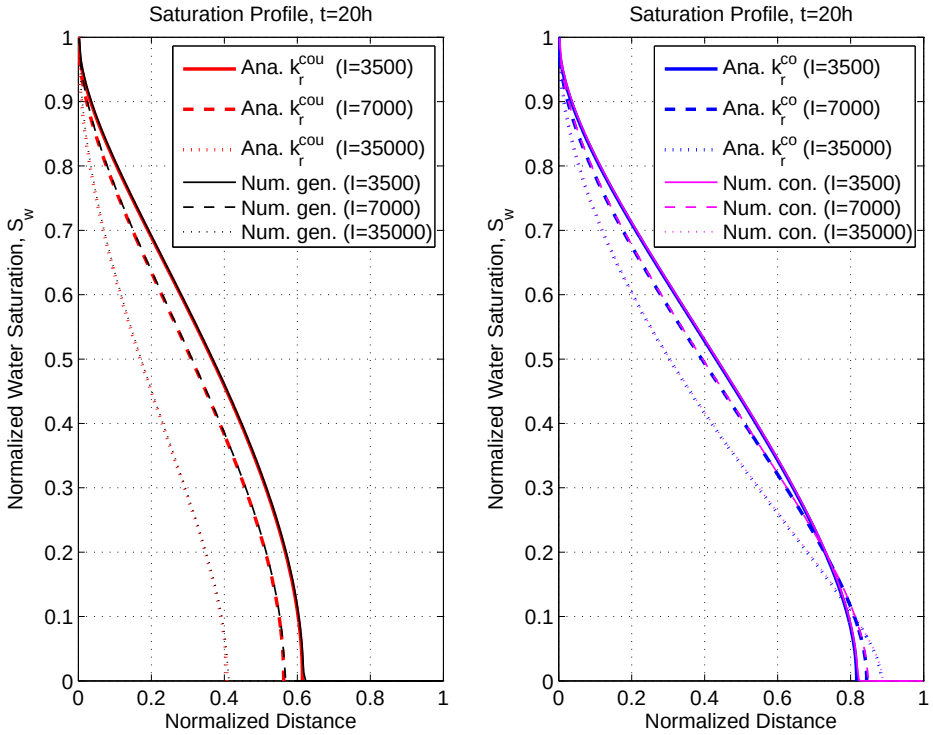

Figure 5.14: Comparison of saturation profiles at t=20 hours. The fluid-fluid interaction parameter I is increased from the base case value of 3500 by factors 2 and 10. Left: Numerical solution of the generalized model and analytical solutions using generalized counter-current relative permeabilities. Right: Numerical solution of the conventional model and analytical solutions using generalized co-current relative permeabilities.

We first note the great match between numerical and analytical solutions for all the values tested here. Secondly, we see that the behaviour of the saturation profiles differ distinctly between the conventional and the generalized solution. For the conventional solution and the matching analytical solution with co-current relative permeabilities we see that increased fluid-fluid interaction leads to a slowdown of the process over most of the mobile saturation range. However, for low saturations ($S_w < 0.15$), the front is actually faster for higher values of I. From Fig. 5.13 we notice that the values of dF/dS at low water saturations are higher when co-current

relative permeabilities are used. Since the position of each saturation depends on the derivative of the fractional flow function, the phenomenon must be caused by changes to the shape of dF/dS (i.e. higher values at low water saturations). The difference in the shape of the derivative curves also explains the more stretched out profiles of the conventional solutions.

For the numerical solution of the generalized model and the matching analytical solution with counter-current relative permeabilities, we have a more uniform slowdown of the imbibition process as the viscous coupling parameter is increased.

5.5.2 Effect of water viscosity

Saturation profiles are again plotted for $t = 20h$ in Fig. 5.15, where we now look at the effect of increasing water viscosity. The base case is plotted for reference, along with solutions where the water viscosity has been increased by factors of 2 and 10. By using the same factors it is also possible to compare the impact of water viscosity against the impact of the fluid-fluid interaction parameter I. It then becomes clear that increasing the water viscosity does more to slow down the process than an equivalent (same factor) increase of I. We also notice that the water viscosity has similar effects for both the generalized and conventional solutions, whereas the response to the fluid-fluid interaction parameter was distinctly different.

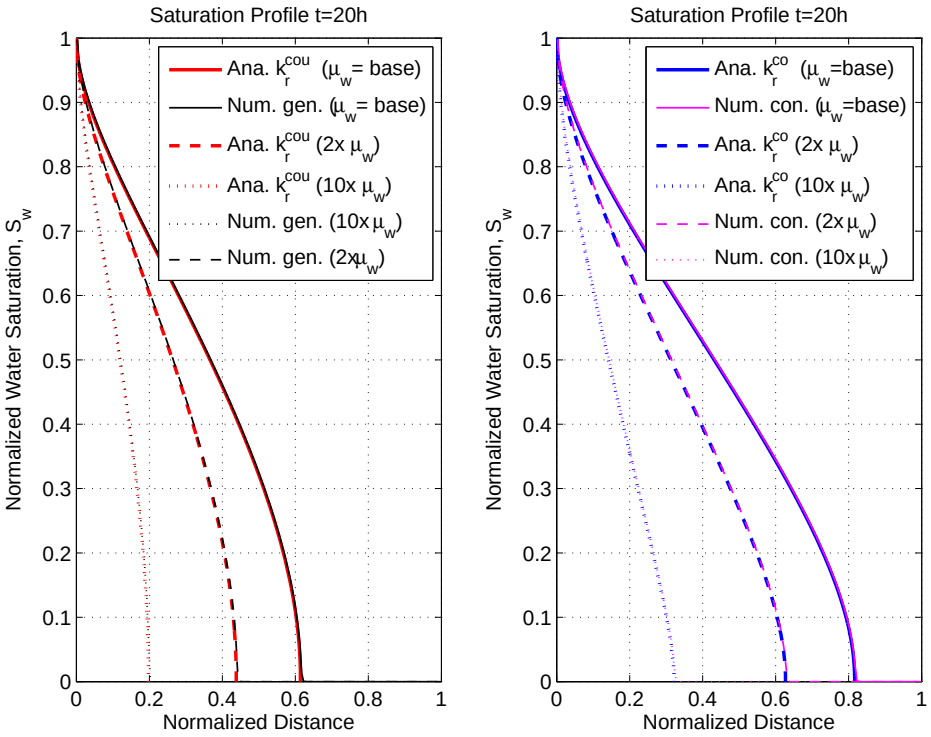

Figure 5.15: Comparison of saturation profiles at t=20 hours. Water viscosity is increased from the base case value of 1.2 mPa·s by factors 2 and 10.

5.5.3 Effect of oil viscosity

Following the same methodology, Fig. 5.16 shows saturation profiles where the oil viscosity has been varied. Clearly, the imbibition process is less sensitive to increases in oil viscosity than to increases in water viscosity, according to both sets of solutions. For the analytical solution with counter-current relative permeabilities and the numerical solution of the generalized model, we note that the response to increased oil viscosity is very similar to the response to increases in I , seen in Fig. 5.14. It should be pointed out that any delay of the saturation front needs to be considered with $\sqrt{t}$ time scaling in mind and is in fact more significant than it might seem at first.

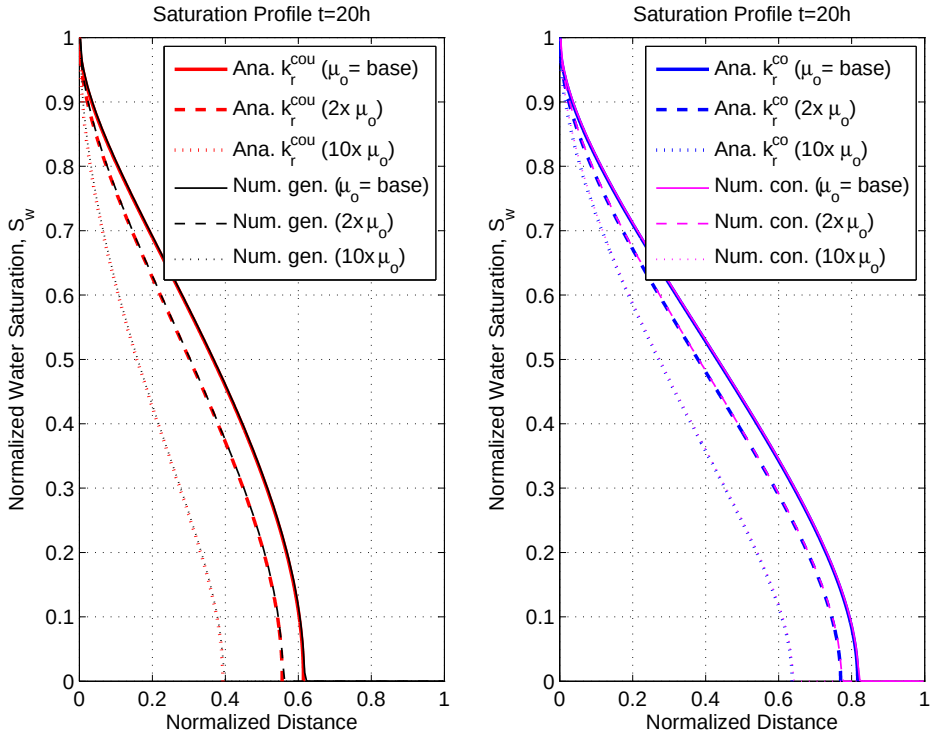

Figure 5.16: Comparison of saturation profiles at t=20 hours. Oil viscosity is increased from the base case value of 1.5 mPa·s by factors 2 and 10.

5.5.4 Oil recovery

Fig. 5.17 displays oil recovery curves, comparing the impact of increasing the fluid-fluid interaction term, water viscosity and oil viscosity. While higher values result in reduced imbibition rates for all these parameters, also here it is seen that increasing the water viscosity leads to the most significant decrease in recovery rate.

For the system considered here, the difference in recovery rate when applying counter-current vs. co-current relative permeabilities is significant for all the tested input parameters. The results are in agreement with previous research, indicating

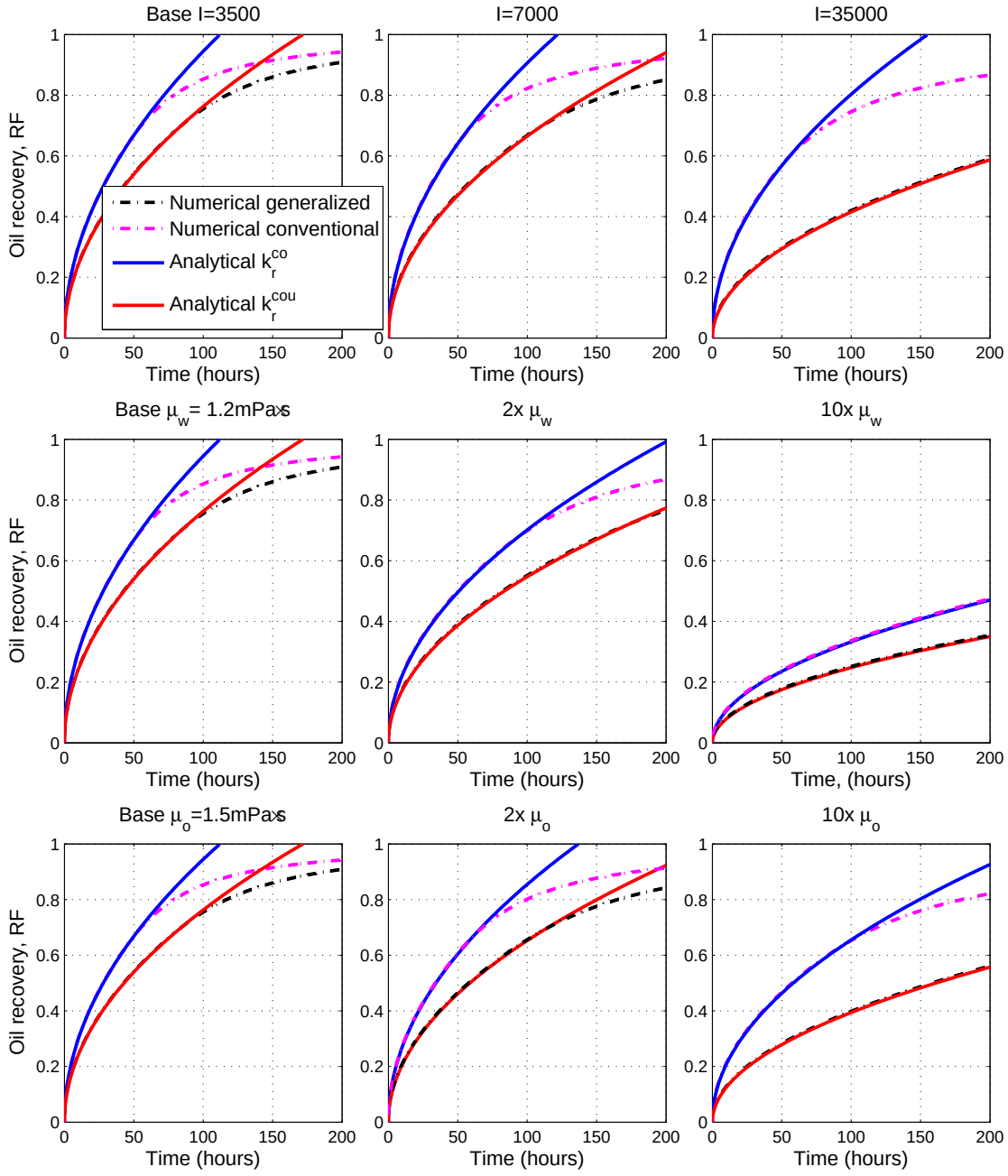

Figure 5.17: Comparison of oil recovery factors ,RF (fraction of mobile oil), corresponding to the cases presented as saturation profiles. Base case is to the left. Parameters are increased towards the right by factors of 2 and 10. Top row: The fluid-fluid interaction term I. Middle row: Water viscosity μ_w. Bottom row: Oil viscosity μ_o.

overestimation of recovery rate if co-current relative permeabilities are used to predict a counter-current SI process (Bourbiaux and Kalaydjian, 1990). By extension, there is also agreement with works showing that co-current SI can be faster and more effective than a counter-current process (Pooladi-Darvish and Firoozabadi,

1998, 2000; Standnes, 2004; Karimaie et al., 2006).

The excellent matches between analytical and numerical solutions suggest that the new generalized relative permeability expressions are able to account for viscous coupling effects seen when the flow mode is changed from co-current to counter-current. It thus seems like the analytical solutions can serve as effective tools in predicting oil recovery for different flow settings, if a set of standard, co-current relative permeabilities is available for matching.

While the results obtained here, together with previous results by Andersen et al. (2019) and Qiao et al. (2018) are definitely encouraging, they are all based on matching parameters to a single set of experiments (Bourbiaux and Kalaydjian, 1990). Further testing should be done by matching parameters to other experiments, particularly with different viscosities and viscosity ratios, but also for varying degree of wettability, as this would likely affect the solid-fluid interaction terms, and therefore also end point relative permeabilities.

Chapter 6

Conclusions

The main goal of this thesis was to incorporate the effects of fluid-fluid interactions (viscous coupling) into analytical solutions for forced and spontaneous imbibition, and to study the the effects of varying degree of fluid-fluid interaction and fluid viscosities for cases corresponding to purely co-current and counter-current flow. A generalized model for two-phase flow, derived from the theory of mixtures (Standnes et al., 2017; Qiao et al., 2018) was applied. The model explicitly accounts for momentum transfer between the two fluids and between fluids and the solid porous medium. It gives rise to generalized relative permeability expressions that depend on fluid-fluid and fluid-solid interaction parameters, as well as fluid viscosities. Input parameters were determined by matching against experimental data from Bourbiaux and Kalaydjian (1990).

In order to incorporate viscous coupling effects into the analytical solution for spontaneous imbibition (McWhorter and Sunada, 1990), a new set of generalized relative permeability expressions has been derived, based on an assumption of purely counter-current flow. The new generalized relative permeabilities for counter-current flow were used to compute the capillary diffusion coefficient, necessary for the analytical solution. For the co-current case, generalized expressions for co-current flow, previously derived in Qiao et al. (2018) and Andersen et al. (2019) were used.

The behaviour of the generalized relative permeabilities was also studied for various values of the input parameters.

The main findings of this work are as follows:

- The generalized relative permeabilities derived under an assumption of counter-current flow will always be lower than the corresponding co-current values if viscous coupling is included ($I \neq 0$). For $I = 0$ both sets reduce to traditional Corey-type expressions.

- The factors relating co- and counter-current relative permeabilities are not constants, but vary with saturation for a given set of input parameters. This is a more complicated relation than what was proposed by Bourbiaux and Kalaydjian (1990).

- Both co- and counter-current relative permeabilities are viscosity-dependent when viscous coupling is assumed (i.e. when $I \neq 0$). Counter-current end point values are sensitive to the viscosity of the opposite phase, while there is no viscosity dependence for the co-current end points.

- The co-current, forced imbibition case was solved by applying generalized co-current relative permeabilities when computing the fractional flow function, which is the main input to the Buckley-Leverett solution. In this case, increased viscous coupling through increases of the fluid-fluid interaction term, I, led to a more efficient displacement process, seen as a higher saturation front and a higher average water saturation behind the front. This is in line with the theory of momentum exchange between the fluid phases, depending on their relative velocities. Increased water viscosity had a similar effect, quickly bringing the process towards a piston-like behaviour. When oil viscosity was increased, the effect was a less effective displacement, seen as a lower front saturation and lower average saturation behind the front. It should be noted that the tests with increased oil viscosity were run with a different saturation exponent for oil, due to the base case value resulting in an unphysical saturation profile. It is thought that the matched saturation exponent was perhaps too high, as it resulted in extreme inflection of the oil relative permeability curve for high oil viscosities.

- For the counter-current SI case, excellent matches between analytical and numerical solutions of both the conventional model and the generalized model based on mixture theory has been obtained. This suggests that the newly derived generalized relative permeability expressions for counter-current flow can be used to predict oil recovery in a counter-current setting if co-current relative permeabilities are known. In this case, increased viscous coupling led to a slowdown of the imbibition process, as both fluids are decelerated when flowing in opposite directions. Similarly, increasing fluid viscosities led to slower imbibition rates, however, for the water-wet system considered here, increases in water viscosity were the most detrimental to the rate of recovery. The observed behaviour is in line with theoretical predictions of the generalized model.

6.1 Suggested future work

- As mentioned in the discussion, the matches obtained between analytical and numerical solutions for the counter-current SI case are encouraging. Still, validation against other experiments is required. For validation, it is suggested that a set of relative permeabilities could be measured for both co-current and counter-current flow, at different fluid viscosities. This would enable matching and direct comparison between experimental and analytically or numerically predicted curves.

- The co-current oil relative permeability that resulted from the combination of the saturation exponent $\beta = 1.5$ and high oil viscosity, proved to be somewhat problematic. More work should be done to understand the role of the saturation exponents, and to perhaps establish some bounds for reasonable values.

References

Abdallah, W., Buckley, J. S., Carnegie, A., Edwards, J., Herold, B., Fordham, E., Graue, A., Habashy, T., Seleznev, N., Signer, C., Hussain, H., Montaron, B., and Ziauddin, M. (2007). Fundamentals of wettability. *Oilfield Review*, 19(2):44–61.

Ambrosi, D. and Preziosi, L. (2002). On the closure of mass balance models for tumor growth. *Mathematical Models and Methods in Applied Sciences*, 12(05):737–754.

Andersen, P., Evje, S., and Kleppe, H. (2014). A model for spontaneous imbibition as a mechanism for oil recovery in fractured reservoirs. *Transport in Porous Media*, 101(2):299–331.

Andersen, P. Ø., Qiao, Y., Standnes, D. C., and Evje, S. (2019). Cocurrent spontaneous imbibition in porous media with the dynamics of viscous coupling and capillary backpressure. *SPE Journal*, 24(01):158–177.

Andersen, P. Ø., Skjæveland, S. M., and Standnes, D. C. (2017a). A novel bounded capillary pressure correlation with application to both mixed and strongly wetted porous media. In *Abu Dhabi International Petroleum Exhibition & Conference*. Society of Petroleum Engineers.

Andersen, P. Ø., Standnes, D. C., and Skjæveland, S. M. (2017b). Waterflooding oil-saturated core samples-analytical solutions for steady-state capillary end effects and correction of residual saturation. *Journal of Petroleum Science and Engineering*, 157:364–379.

Anderson, W. G. (1987). Wettability literature survey part 5: the effects of wettability on relative permeability. *Journal of Petroleum Technology*, 39(11):1–453.

Armstrong, R. T., McClure, J., Berill, M., Rücker, M., Schlüter, S., and Berg, S. (2017). Flow regimes during immiscible displacement. *Petrophysics*, 58(01):10–18.

Avraam, D. and Payatakes, A. (1995a). Flow regimes and relative permeabilities during steady-state two-phase flow in porous media. *Journal of Fluid Mechanics*, 293:207–236.

Avraam, D. and Payatakes, A. (1995b). Generalized relative permeability coefficients during steady-state two-phase flow in porous media, and correlation with the flow mechanisms. *Transport in Porous Media*, 20(1-2):135–168.

Babchin, A., Yuan, J., and Nasr, T. (1998). Generalized phase mobilities in gravity drainage processes. In *Annual Technical Meeting*. Petroleum Society of Canada.

Bear, J. (2013). *Dynamics of fluids in porous media*. Courier Corporation.

Bentsen, R. and Manai, A. (1992). Measurement of cocurrent and countercurrent relative permeability curves using the steady-state method. *AOSTRA J. Res*, 7:169–181.

Bourbiaux, B. J. and Kalaydjian, F. J. (1990). Experimental study of cocurrent and countercurrent flows in natural porous media. *SPE Reservoir Engineering*, 5(03):361–368.

Bowen, R. M. (1980). Incompressible porous media models by use of the theory of mixtures. *International Journal of Engineering Science*, 18(9):1129–1148.

Brooks, R. and Corey, A. (1964). Hydraulic properties of porous media. *Hydrology Papers, No. 3, Colorado State University*.

Buckley, S. E. and Leverett, M. C. (1942). Mechanism of fluid displacement in sands. *Transactions of the AIME*, 146(01):107–116.

Chen, Z.-X. (1988). Some invariant solutions to two-phase fluid displacement problems including capillary effect. *SPE Reservoir Engineering*, 3(02):691–700.

Craig, F. F. (1971). *The reservoir engineering aspects of waterflooding*, volume 3. HL Doherty Memorial Fund of AIME New York.

Dake, L. P. (1983). *Fundamentals of reservoir engineering*, volume 8. Elsevier.

Darcy, H. P. G. (1856). *Les Fontaines publiques de la ville de Dijon. Exposition et application des principes à suivre et des formules à employer dans les questions de distribution d'eau, etc.* Paris: V. Dalamont.

Dullien, F. and Dong, M. (1996). Experimental determination of the flow transport coefficients in the coupled equations of two-phase flow in porous media. *Transport in Porous Media*, 25(1):97–120.

Ehrlich, R. (1993). Viscous coupling in two-phase flow in porous media and its effect on relative permeabilities. *Transport in Porous Media*, 11(3):201–218.

Fokas, A. and Yortsos, Y. (1982). On the exactly solvable equation s_t=(βs+γ)ˆ-2s_x_x+α(βs+γ)ˆ-2s_x occurring in two-phase flow in porous media. *SIAM Journal on Applied Mathematics*, 42(2):318–332.

Geffen, T., Owens, W. W., Parrish, D., and Morse, R. (1951). Experimental investigation of factors affecting laboratory relative permeability measurements. *Journal of Petroleum Technology*, 3(04):99–110.

Helmig, R. (1997). *Multiphase flow and transport processes in the subsurface: a contribution to the modeling of hydrosystems.* Springer-Verlag.

Honarpour, M. and Mahmood, S. (1988). Relative-permeability measurements: An overview. *Journal of petroleum technology*, 40(08):963–966.

Honarpour, M. M., Huang, D., and Dogru, A. (1996). Simultaneous measurements of relative permeability, capillary pressure, and electrical resistivity with microwave system for saturation monitoring. *SPE Journal*, 1(03):283–294.

Karimaie, H., Torsæter, O., Esfahani, M., Dadashpour, M., and Hashemi, S. (2006). Experimental investigation of oil recovery during water imbibition. *Journal of Petroleum Science and Engineering*, 52(1-4):297–304.

Kashchiev, D. and Firoozabadi, A. (2003). Analytical solutions for 1d countercurrent imbibition in water-wet media. *SPE Journal*, 8(04):401–408.

Lefebvre du Prey, E. (1973). Factors affecting liquid-liquid relative permeabilities of a consolidated porous medium. *Society of Petroleum Engineers Journal*, 13(01):39–47.

Leverett, M. (1941). Capillary behavior in porous solids. *Transactions of the AIME*, 142(01):152–169.

Li, Y., Morrow, N. R., and Ruth, D. (2003). Similarity solution for linear countercurrent spontaneous imbibition. *Journal of Petroleum Science and Engineering*, 39(3-4):309–326.

Lucas, R. (1918). Ueber das zeitgesetz des kapillaren aufstiegs von flüssigkeiten. *Colloid & Polymer Science*, 23(1):15–22.

March, R., Doster, F., and Geiger, S. (2016). Accurate early-time and late-time modeling of countercurrent spontaneous imbibition. *Water Resources Research*, 52(8):6263–6276.

Mason, G. and Morrow, N. R. (2013). Developments in spontaneous imbibition and possibilities for future work. *Journal of Petroleum Science and Engineering*, 110:268–293.

McWhorter, D. B. and Sunada, D. K. (1990). Exact integral solutions for two-phase flow. *Water Resources Research*, 26(3):399–413.

Muskat, M., Wyckoff, R., Botset, H., and Meres, M. (1937). Flow of gas-liquid mixtures through sands. *Transactions of the AIME*, 123(01):69–96.

Nejad, K. S., Berg, E. A., and Ringen, J. K. (2011). Effect of oil viscosity on water/oil relative permeability. In *International symposium of the society of core analysts, Austin, TX, USA*. Society of Core Analysts.

Nooruddin, H. A. and Blunt, M. J. (2016). Analytical and numerical investigations of spontaneous imbibition in porous media. *Water Resources Research*, 52(9):7284–7310.

Odeh, A. S. (1959). Effect of viscosity ratio on relative permeability. *Transactions of the AIME*, 213:346–352.

Onsager, L. (1931). Reciprocal relations in irreversible processes. i. *Physical Review*, 37(4):405.

Philip, J. (1960). A very general class of exact solutions in concentration-dependent diffusion. *Nature*, 185(4708):233.

Pooladi-Darvish, M. and Firoozabadi, A. (1998). Experiments and modelling of water injection in water-wet fractured porous media. In *Annual Technical Meeting*. Petroleum Society of Canada.

Pooladi-Darvish, M. and Firoozabadi, A. (2000). Cocurrent and countercurrent imbibition in a water-wet matrix block. *SPE Journal*, 5(01):3–11.

Preziosi, L. and Farina, A. (2002). On darcy's law for growing porous media. *International Journal of Non-Linear Mechanics*, 37(3):485–491.

Qiao, Y., Andersen, P., Evje, S., and Standnes, D. (2018). A mixture theory approach to model co-and counter-current two-phase flow in porous media accounting for viscous coupling. *Advances in Water Resources*, 112:170–188.

Rajagopal, K. and Tao, L. (1995). *Mechanics of mixtures*. World Scientific.

Rapoport, L. and Leas, W. (1953). Properties of linear waterfloods. *Journal of Petroleum Technology*, 5(05):139–148.

Richardson, J., Kerver, J., Hafford, J., and Osoba, J. (1952). Laboratory determination of relative permeability. *Journal of Petroleum Technology*, 4(08):187–196.

Schmid, K. and Geiger, S. (2012). Universal scaling of spontaneous imbibition for water-wet systems. *Water Resources Research*, 48(3).

Schmid, K. and Geiger, S. (2013). Universal scaling of spontaneous imbibition for arbitrary petrophysical properties: Water-wet and mixed-wet states and handy's conjecture. *Journal of Petroleum Science and Engineering*, 101:44–61.

Schmid, K. S., Geiger, S., and Sorbie, K. S. (2011). Semianalytical solutions for cocurrent and countercurrent imbibition and dispersion of solutes in immiscible two-phase flow. *Water Resources Research*, 47(2).

Standnes, D. C. (2004). Experimental study of the impact of boundary conditions on oil recovery by co-current and counter-current spontaneous imbibition. *Energy & Fuels*, 18(1):271–282.

Standnes, D. C. and Andersen, P. Ø. (2017). Analysis of the impact of fluid viscosities on the rate of countercurrent spontaneous imbibition. *Energy & Fuels*, 31(7):6928–6940.

Standnes, D. C., Evje, S., and Andersen, P. Ø. (2017). A novel relative permeability model based on mixture theory approach accounting for solid–fluid and fluid–fluid interactions. *Transport in Porous Media*, 119(3):707–738.

Wang, J., Dong, M., and Asghari, K. (2006). Effect of oil viscosity on heavy oil-water relative permeability curves. In *SPE/DOE Symposium on Improved Oil Recovery*. Society of Petroleum Engineers.

Washburn, E. W. (1921). The dynamics of capillary flow. *Physical Review*, 17(3):273.

Yuster, S. (1951). Theoretical considerations of multiphase flow in idealized capillary systems. In *Proceedings of the Third World Petroleum Congress*, volume 2, pages 437–445. E. Brill The Hague.

Nomenclature

α, β Water/oil-interaction saturation exponents

$\hat{\lambda}_o, \hat{\lambda}_w$ Generalized phase mobilities ($m^2/(Pa \cdot s)$)

$\hat{\lambda}_T$ Generalized total mobility ($m^2/(Pa \cdot s)$)

$\hat{\lambda}_{oo}, \hat{\lambda}_{ww}$ Generalized diagonal mobilities ($m^2/(Pa \cdot s)$)

$\hat{\lambda}_{ow}, \hat{\lambda}_{wo}$ Generalized cross-term mobilities ($m^2/(Pa \cdot s)$)

$\hat{k}_{ri}^{cou}$ Generalized counter-current relative permeability for phase i

$\hat{k}_{ri}^{co}$ Generalized co-current relative permeability for phase i

λ_o, λ_w Phase mobilities ($m^2/(Pa \cdot s)$)

λ_T Total mobility ($m^2/(Pa \cdot s)$)

μ_o Oil viscosity ($Pa \cdot s$)

μ_w Water viscosity ($Pa \cdot s$)

ϕ Standard porosity

ϕ_e Effective porosity

ρ Density (kg/m^3)

σ_{ow} Oil/water interfacial tension (N/m)

θ Contact angle related to wettability

A Inflow parameter controlling rate of SI ($ms^{-1/2}$)

a_1, a_2, c, k_1, k_2 Capillary pressure correlation parameters for J-function

A_c Cross-sectional area (m^2)

C_o Oil counter-current factor, $C_o = \hat{k}_{ro}^{cou} \ / \ \hat{k}_{ro}^{co}$

C_w Water counter-current factor, $C_w = \hat{k}_{rw}^{cou} \ / \ \hat{k}_{rw}^{co}$

D Capillary duffusion coefficient (m^2/s)

F	Fractional flow function for capillary flow
f	Fractional flow function without capillary pressure
I	Oil/water interaction parameter $(\mathrm{Pa} \cdot \mathrm{s})^{-1}$
I_o	Oil/solid interaction parameter
I_w	Water/solid interaction parameter
J	Dimensionless Leverett J-function for capillary pressure
k	Absolute permeability (m^2)
k_{ro}	Oil relative permeability
k_{ro}^{max}	Oil end point relative permeability
k_{rw}	Water relative permeability
k_{rw}^{max}	Water end point relative permeability
L	Length of reservoir or core sample (m)
n_o	Corey exponent for oil
n_w	Corey exponent for water
p_c	Capillary pressure (Pa)
p_o	Oil phase pressure (Pa)
p_w	Water phase pressure (Pa)
Q	Injection rate (m^3/s)
$Q_w(t)$	Cumulative 1D volume of water imbibed (m)
R	Oil/water interaction term $(\mathrm{Pa} \cdot \mathrm{s}/\mathrm{m}^2)$
R_o	Oil/solid interaction term $(\mathrm{Pa} \cdot \mathrm{s}/\mathrm{m}^2)$
R_w	Water/solid interaction term $(\mathrm{Pa} \cdot \mathrm{s}/\mathrm{m}^2)$
RF	Recovery factor of mobile oil
s_0	Wetting phase saturation at inlet (x=0)
S_f	Normalized front saturation
s_i	Initial wetting phase saturation
S_o	Normalized oil saturation

s_o	Oil saturation
S_w	Normalized water saturation
s_w	Water saturation
s_{or}	Oil residual saturation
s_{wr}	Water residual saturation
T	Dimensionless time in Buckley-Leverett solution
t	Time (s)
t^*	Time when analytical solutions for SI stop being valid (s)
T_{bt}	Dimensionless time at water breakthrough
u_0	Maximum water flux or Darcy velocity during SI (m/s)
u_o	Oil flux or Darcy velocity (m/s)
u_T	Total flux or Darcy velocity (m/s)
u_w	Water flux or Darcy velocity (m/s)
V	Volume of control element (m^3)
v_o	Oil interstitial velocity (m/s)
v_w	Water interstitial velocity (m/s)
W	Generalized mobility term for capillary diffusion ($m^2/(Pa \cdot s)$)
x	Spatial coordinate along reservoir/core (m)

Appendices

1 Matlab code for Buckley-Leverett case

```
% Solution of Buckley Leverett with viscous coupling
% through generalized relative permeabilities.

clear all

% Input
swi = 0.4;                  % Irreducible water sat.
sor = 0.425;                % Irreducible oil sat.
L = 0.29;                   % Core length (m)
phi = 0.233;                % Porosity
K = 1.18e-13;               % Absolute permeeability (m^2)

% Time (dimensionless)
T = 0.7;                    % Equals Pore Volumes

% Interaction parameters
Iw = 23.26;                 % Solid-water
Io = 2.15;                  % Solid-oil
I = 3500;                   % Oil-water

% Saturation exponents
alpha = -0.2;                % Water
beta = 1.5;                  % Oil

% Viscosities
muo = 1.5*0.001             % Oil (Pa*s)
muw = 1.2*0.001             % Water (Pa*s)
M = muw/muo                 % Viscosity ratio

% Saturation vector
Sstep = 0.0001;
S = 0:Sstep:1;              % S is normalized
s = swi+ S*(1-sor-swi); % s is not

% Get generalized kr curves
[krw_co, kro_co, krw_cou, kro_cou, cfw, cfo] = ...
    relperm_gen(S, muw, muo, K, Iw, Io, I, alpha, beta);

% End points
kro_end = 1/Io;
krw_end = 1/Iw;
```

```
% Check mobility ratios
mobrat = (krw_end/muw)/(kro_end/muo);   % End point ratio
mobrats = (krw_co/muw)./(kro_co/muo);

% Compute fractional flow function
f = ((1+(kro_co./krw_co)*(muw/muo)).^(-1));

% Compute derivative of fractional flow function
df= gradient(f)./gradient(S);


% Plot rel. perm.
subplot(2,2,1)
plot(S,krw_co,'-r','LineWidth',2,'DisplayName','k_{rw}^{
   co}');hold on
plot(S,kro_co,'-b','LineWidth',2,'DisplayName','k_{ro}^{
   co}');hold on
grid on
title('Relative Permeability','FontSize',12)
xlabel('Normalized Water Saturation','FontSize',12)
ylabel('kr, fraction','FontSize',12)
legend('-DynamicLegend')

% Plot fractional flow function f(S)
subplot(2,2,2)
plot(S,f,'-r','LineWidth',2);hold on
title('Fractional Flow Function','FontSize',12)
xlabel('Normalized Water Saturation','FontSize',12)
ylabel('f(S)','FontSize',12)
grid on
hold on

% Plot f'(S)
subplot(2,2,4)
plot(S,df,'--r','LineWidth',2);hold on
title('df/dS and g','FontSize',12)
xlabel('Normalized Water Saturation','FontSize',12)
ylabel('','FontSize',12)
hold on
grid on

% Function g for finding front saturation
g=df-(f./S);
```

```
% If no root is found for g, plot lines for piston-like
   displacement
if min(g)>=0
    'g has no nontrivial root'
    subplot(2,2,3)
    line([T;T],[1;0],'LineWidth',2);
    line([0;T],[1;1],'LineWidth',2);
    title('Saturation Profile','FontSize',12)
    xlabel('Dimensionless Distance','FontSize',12)
    ylabel('Normalized Water Saturation','FontSize',12)
    axis([0 1 0 1])
    grid on
    hold on

    subplot(2,2,4)
    plot(S,g,'-b','LineWidth',2)
    ylabel('Values','FontSize',12)
    legend('df/dS','g=(df/dS)*S-f(S)')
return
end

% Plot g
plot(S,g,'-b','LineWidth',2)
ylabel('Values','FontSize',12)
legend('df/dS','g=(df/dS)*S-f(S)')

% Find last positive g
for i=1:1:length(g)-1
    x1=g(i);
    x2=g(1+i);
    prod=x1*x2;
    if prod<0
        gzero=i
        break
    else i=i+1;
    end
end

% Front saturation, Sf
Sf=S(gzero)

% Position of front, xf
xpos = (df.*T);
xf = xpos(gzero)
```

```
% Position of saturations above (behind) front saturation
SS=Sf:Sstep:1;
XX=xpos([gzero:end]);

% Plot solution
subplot(2,2,3)
title('Saturation Profile','FontSize',12)
xlabel('Dimensionless Distance','FontSize',12)
ylabel('Normalized Water Saturation','FontSize',12)
axis([0 1 0 1])
grid on
hold on
plot(XX,SS,'-b','LineWidth',2)
line([xf;xf],[0;Sf],'LineWidth',2);

% Oilrecovery %
% Time for water breakthrough
Tend = 1/df(gzero)

% If T >= Tend, find Sstar, the water saturation that has
    been transported
% a distance x=1 for the given T

if T<Tend
    RF = T
else
% Find saturation that has reached x=1
    for j=1:length(XX)
        if XX(j)<=1
            index=j
            Sstar=S(gzero+index)
        break
        end

    end
% Recovery after breakthrough
    RF = Sstar + T*(1 - f(gzero+index))
end
```

2 Matlab code for generalized relative permeabilities

```
function [krw_co, kro_co, krw_cou, kro_cou, cfw, cfo] =
   relperm_gen(S, muw, muo, K, Iw, Io, I, alpha, beta)

krw_co   = zeros(size(S));
kro_co   = zeros(size(S));

%Co-current part
krw_co = (Io.*S.*(1-S).^(beta-1) + I*muw.*S)./(Iw*Io.*S
   .^(alpha-1).*(1-S).^(beta-1) + I.*(Iw.*S.^(alpha)*muw
   + Io.*(1-S).^(beta)*muo));
kro_co = (Iw.*(1-S).*S.^(alpha-1) + I*muo.*(1-S))./(Iw*Io
   .*S.^(alpha-1).*(1-S).^(beta-1) + I.*(Iw.*S.^(alpha)*
   muw + Io.*(1-S).^(beta)*muo));

%Cocurrent Endpoints
krw_co(1) = 0;
krw_co(end) = 1/Iw;
kro_co(1 )= 1/Io;
kro_co(end) = 0;

%Counter-current factors
cfw = ((Io.*(1-S).^(beta-1) + I.*S*muw)./(Io.*(1-S).^(
   beta-1) + I.*S*muw + I.*(1-S)*muw)) - ((I.*S.*(1-S)*
   muo)./(Iw.*S.^(alpha-1) + I.*(1-S)*muo + I.*S.*(1-S)*
   muo));
cfo = ((Iw.*S.^(alpha-1) + I.*(1-S)*muo)./(Iw.*S.^(alpha
   -1) + I.*(1-S)*muo + I.*S*muo)) - ((I.*S.*(1-S)*muw)
   ./(Io.*(1-S).^(beta-1) + I.*S*muw + I.*S.*(1-S)*muw));

%Countercurrent factors at endpoints
cfw(1) = Io/(Io+I*muw);          %Water factor at Sw=0
cfw(end)= Iw/(Iw+I*muo);         %Water factor at Sw=1
cfo(1)= Io/(Io+I*muw);           %Oil factor at Sw=0
cfo(end)= Iw/(Iw+I*muo);         %Oil factor at Sw=1

%Countercurrent curves
krw_cou = krw_co.*cfw;
kro_cou = kro_co.*cfo;

end
```

3 Matlab code for counter-current SI case

Main script

```
% This script gets values for A and dF for both sets of
   relative
% permeabilities from the functions CCSIco and
   CCSIcounter and is
% used to calculate and plot saturation profiles and oil
   recovery.

clear

% Input
swi = 0.4;                % Irreducible water sat.
sor = 0.425;              % Irreducible oil sat.
L = 0.29;                 % Core length (m)
phi = 0.233;              % Porosity
K = 1.18e-13;             % Absolute permeability (m^2)
sigma = 15.8*0.001;       % IFT (N/m)


si = swi;      % Initial water saturation = irreducible
s0 = 1-sor;    % Water saturation at inlet

% Calculate recovery at these times (seconds)
times = [0.0001 0.001 0.005 0.01 0.05 0.1 0.3 0.5 0.7 0.9
    1:1:200]*3600;
% Interaction parameters

Iw = 23.26
Io = 2.15
I = 3500

% Saturation exponents
alpha = -0.2                    %water
beta = 1.5                     %oil

% Viscosities
muo = 1*1.5*0.001             %Pa.s
muw = 1*1.2*0.001             %Pa.s

M = muw/muo
```

```
% Saturation vector
Sstep = 0.001;
S = 0:Sstep:1;                % Capital S is normalized
s = swi+ S*(1-sor-swi);

% Get values of A and F'(S) for co- and counter-current
   rel-perms.
[A_co, dF_co] = CCSIco(K, sigma, phi, swi, sor, muw, muo,
    M, alpha, beta, Iw, Io, I, S, s, L, si, s0, Sstep);
[A_cou, dF_cou] = CCSIcounter(K, sigma, phi, swi, sor,
   muw, muo, M, alpha, beta, Iw, Io, I, S, s, L, si, s0,
   Sstep);

n=1;
for t=times;

% Find x-position of saturations after time t
% For kr_co
x_co=(2*A_co/phi)*dF_co*t^(1/2);
xd_co=x_co/L;      %Normalized length

% For kr_cou
x_cou=(2*A_cou/phi)*dF_cou*t^(1/2);
xd_cou=x_cou/L;    %Normalized length


%  Oil recovery, RF, fraction of mobile oil (strictly
   only valid before
%  front reaches boundary, as the solution is based on an
    infinite medium).

% RF from numerical integration of saturation profile
RFco(n)= trapz(s,xd_co)/(1-sor-swi);
RFcou(n)= trapz(s,xd_cou)/(1-sor-swi);

% RF from total volume imbibed
VRFco(n)= 2*A_co*t^0.5/(L*phi*(1-sor-swi));
VRFcou(n)= 2*A_cou*t^0.5/(L*phi*(1-sor-swi));



% Plot saturation profiles at these times
if t==20*3600
figure(2)
```

```
subplot(1,3,1)
plot(xd_co,S,'-b','LineWidth',2);hold on
plot(xd_cou,S,'-r','LineWidth',2)
title('Saturation Profile')
xlabel('Dimensionless Distance')
ylabel('Normalized Water Saturation')
grid on
hold on
end

if t==50*3600
figure(2)
subplot(1,3,2)
plot(xd_co,S,'-b','LineWidth',2);hold on
plot(xd_cou,S,'-r','LineWidth',2)
title('Saturation Profile')
xlabel('Dimensionless Distance')
ylabel('Normalized Water Saturation')
grid on
hold on

end
if t==100*3600
figure(2)
subplot(1,3,3)
plot(xd_co,S,'-b','LineWidth',2);hold on
plot(xd_cou,S,'-r','LineWidth',2)
title('Saturation Profile')
xlabel('Dimensionless Distance')
ylabel('Normalized Water Saturation')
% axis([0 1 0 1])
grid on
hold on

end

n=n+1;

end


% Find t*, time when front reaches end and solution stops
    being valid.
% For kr_co
  tstar_co = (L*phi/(2*A_co.*dF_co(1))).^2/3600     %
```

```
    Hours

% For kr_cou
  tstar_cou = (L*phi/(2*A_cou.*dF_cou(1))).^2/3600  %
    Hours

% Plot oil recovery RF
figure(1)
hold on
subplot(2,4,[7,8])
plot(times/3600,RFco,'-b','LineWidth',2,'DisplayName','
   Analytical k_r^{co}');hold on
plot(times/3600,RFcou,'-r','LineWidth',2,'DisplayName','
   Analytical k_r^{cou}')
xlabel('Time (hours)')
ylabel('Recovery Factor, fraction of mobile oil')
legend('-DynamicLegend')
hold on
grid on
% Saturation profile at last time
figure(1)
subplot(2,4,4)
plot(xd_co,S,'-b','LineWidth',2);hold on
plot(xd_cou,S,'-r','LineWidth',2)
title('Saturation Profile')
xlabel('Dimensionless distance, fraction')
ylabel('Normalized water saturation')
% axis([0 1 0 1])
grid on
hold on
```

Capillary pressure function

```
function [ Pc ] = Capillary(S,sigma, phi, K)

a1 = .56;
a2 = .66;
c  = .55;
k1 = 1.25;
k2 = 0.08;

 Pc = (a1./(1+k1*S)-a2./(1+k2*(1-S))+c)*sigma*(phi/K)
    ^0.5;
end
```

Computation of co-current A, F(S) and F'(S)

```
function [A,dF] = CCSIco(K, sigma, phi, swi, sor, muw,
   muo, M, alpha, beta, Iw, Io, I, S, s, L, si, s0, Sstep
   )

% Get capillary pressure curve
Pc = Capillary(S,sigma, phi, K);
% Capillary pressure gradient
dPc = gradient(Pc)./gradient(s);

% Get rel. perm.
[krw_co, kro_co, krw_cou, kro_cou, cfw, cfo] =
   relperm_gen(S, muw, muo, K, Iw, Io, I, alpha, beta)

% Capillary Diffusion coefficient
D = -K.*kro_co/muo.*((1+(kro_co./krw_co)*(muw/muo)).^(-1)
   ).*dPc;    %Cocurrent

%Find F iteratively
maxerror = 10                %Error measure to determine
   convergence.
Fold = ones(size(s));        %Start with guessing F(s)=1
   for all saturations.
i=0;                         %Iteration counter.


while maxerror > 0.0001      %Iterate until difference
   between successive F is less than the specified
   condition.

for n = 1:length(s)
    sw = s(n);

    %Find int1, the integral from sw to s0 of (s-sw).*D(s
       )./F(s) ds
    Sindex1= s<=s0 & s>=sw;

    fun1 = ((s-sw).*D.*Sindex1./Fold);
    fun1(isnan(fun1))=0;
    int1 = trapz(s,fun1);

    %Find int2, the integral from si to s0 of (s-s0).*D(s
       )./F(s) ds
    Sindex2= s<=s0 & s>=si;
```

```
    fun2 = ((s-si).*D.*Sindex2./Fold);
    fun2(isnan(fun2))=0;
    int2 = trapz(s,fun2);

    Fnew(n) = 1 - (int1/int2);
end

maxerror=max(abs(1-(Fnew./Fold)));

Fold=Fnew;

i=i+1;

errors(i)=maxerror;
end
errors
iterations=i

% Find F'
% Numerical differentiation
dF = gradient(Fnew)./gradient(s);

% Calculate A for co-current relperm
Sindex3= s<=s0 & s>=si;

fun3 = ((s-si).*D.*Sindex3./Fnew);
fun3(isnan(fun3))=0;
int3 = trapz(s,fun3);

A = sqrt((phi/2)*int3)

end
```

Computation of counter-current A, F(S) and F'(S)

```
function [A,dF] = CCSIcounter(K, sigma, phi, swi, sor,
   muw, muo, M, alpha, beta, Iw, Io, I, S, s, L, si, s0,
   Sstep)

% Get capillary pressure curve
Pc = Capillary(S,sigma, phi, K);
% Capillary pressure gradient
dPc = gradient(Pc)./gradient(s);

% Get rel. perm.
[krw_co, kro_co, krw_cou, kro_cou, cfw, cfo] =
   relperm_gen(S, muw, muo, K, Iw, Io, I, alpha, beta)

% Capillary Diffusion coefficient
D = -K.*kro_cou/muo.*((1+(kro_cou./krw_cou)*(muw/muo))
   .^(-1)).*dPc;    %Countercurrent

%Find F iteratively
maxerror = 10                %Error measure to determine
   convergence.
Fold = ones(size(s));        %Start with guessing F(s)=1
   for all saturations.
i=0;                         %Iteration counter.
while maxerror > 0.0001      %Iterate until difference
   between successive F is less than the specified
   condition.

for n = 1:length(s)
    sw = s(n);

    %Find int1, the integral from sw to s0 of (s-sw).*D(s
       )./F(s) ds
    Sindex1= s<=s0 & s>=sw;

    fun1 = ((s-sw).*D.*Sindex1./Fold);
    fun1(isnan(fun1))=0;
    int1 = trapz(s,fun1);

    %Find int2, the integral from si to s0 of (s-s0).*D(s
       )./F(s) ds
    Sindex2= s<=s0 & s>=si;

    fun2 = ((s-si).*D.*Sindex2./Fold);
```

```
    fun2(isnan(fun2))=0;
    int2 = trapz(s,fun2);

    Fnew(n) = 1 - (int1/int2);
end

maxerror=max(abs(1-(Fnew./Fold)));

Fold=Fnew;

i=i+1;

errors(i)=maxerror;
end
errors
iterations=i

% Find F'
% Numerical differentiation
dF = gradient(Fnew)./gradient(s);

% Calculate A for couunter-current relperm
Sindex3= s<=s0 & s>=si;

fun3 = ((s-si).*D.*Sindex3./Fnew);
fun3(isnan(fun3))=0;
int3 = trapz(s,fun3);

A = sqrt((phi/2)*int3)
end
```